

1 Improving fluid flow in geothermal reservoirs by thermal and mechanical stimulation:  
2 The case of Krafla volcano, Iceland

3 **G. H. Eggertsson<sup>1\*</sup>, Y. Lavallée<sup>1</sup>, J. E. Kendrick<sup>1</sup>, S. H. Markússon<sup>2</sup>**

4 <sup>1</sup>Department of Earth, Ocean and Ecological Sciences, University of Liverpool, 4 Brownlow Street,  
5 Liverpool, United Kingdom, L69 3GP

6 <sup>2</sup>Landsvirkjun, Háaleitisbraut 68, 110 Reykjavík, Iceland

7 \*g.eggertsson@liverpool.ac.uk

8

9 **ABSTRACT**

10 The magmatic-hydrothermal system at Krafla Volcano, North-East Iceland, is an important source of  
11 fluids exploited for geothermal energy. Here, we employ laboratory measurements to constrain the  
12 porosity and permeability of the main lithologies forming the reservoir, and investigate the impacts of  
13 different thermal and mechanical stimulation practices to improve fluid flow.

14

15 Six main rock types were identified and sampled: three basalts (a dense and a porous lava, and a  
16 surficial dyke); a hyaloclastite; an obsidian; an ignimbrite; a felsite; and a gabbro. Permeability  
17 measurements were made in a hydrostatic cell using the steady-state flow method at a range of  
18 confining pressures (1-100 MPa). The measurements show that permeability generally increases with  
19 porosity, but that permeability may vary significantly for a given porosity, depending on the presence  
20 of pore connectivity and micro-fractures. We note that an increase in effective pressure results in a  
21 decrease in permeability due to closure of pre-existing cracks, abundant in some rocks. When  
22 unloading, samples fail to recover pre-loading permeability, as cracks do not necessarily entirely  
23 reopen. To further examine the hysteresis imposed by crack closure, we cyclically loaded/ unloaded a  
24 felsite sample ten times by varying pore pressure which resulted in a further nonlinear decreases in  
25 permeability with each pressurisation cycle; thus an understanding of the pressurisation path may be a  
26 requirement to constrain fluid flow variations in geothermal systems.

27

28 To test the effects of thermal stimulation on fluid flow, samples of dense basalt and felsite were  
29 thermally stressed by heating to 450 °C and cooling at different rates (in air, in water and at a  
30 controlled rate of  $<5 \text{ }^\circ\text{C}\cdot\text{min}^{-1}$ ). The results show that the permeability of originally highly fractured  
31 rocks is not affected by thermal stressing, but originally unfractured rocks show a nonlinear increase in  
32 permeability with each thermal stressing cycle, especially with the largest thermal shock imposed by  
33 quenching in water; thus thermal stimulation may not be expected to result in a similar magnitude of  
34 permeability creation along the length of a borehole.

35

36 Finally, following the permeability measurements on intact rocks, the Brazilian tensile testing method  
37 was employed to impart one and two (orthogonal) macro-fractures, and permeability was measured  
38 after each step. The creation of one macro-fracture strongly enhanced the permeability of the rock  
39 (especially dense rocks), resulting in a narrower range of permeability (as a function of porosity) for  
40 the fractured rocks. Imparting a second fracture had trivial additional impact on the permeability of the  
41 rock. Yet, the presence of fine fragments and possible minor offset of fracture interfaces was found to  
42 obstruct fracture closure, which resulted in higher permeability irrespective of effective pressure; thus  
43 hydraulic fracturing may locally increase fluid flow, especially when employing proppants to obstruct  
44 fracture closure and ensure a stable permeable network in a reservoir.

45

46 We discuss the implications of the findings for a first order constraint on the permeability of the  
47 reservoir rock and the potential of thermal and mechanical stimulation methods on energy production  
48 in geothermal systems nested in active volcanic fields.

49

## 50 **1 Introduction**

### 51 **1.1 Fluid flow in reservoirs**

52 Fluid flow in geomaterials has been the subject of numerous studies since the pioneering efforts of  
53 Henry Darcy (Darcy, 1856; Darcy, 1857). These studies have highlighted the central importance of  
54 fluid flow in many environments, namely: water aquifers (e.g. Strehlow et al., 2015), petroleum and  
55 gas reservoirs (e.g. Jansen, 2011), volcanoes (e.g. Edmonds and Herd, 2007), and hydrothermal

56 systems utilised for geothermal energy (e.g. Darling and Armannsson, 1989) – the subject of this  
57 study.

58

59 Hydrothermal systems are widespread on Earth and whilst they have been utilised for their thermal  
60 output in many cultures (e.g. Carlino et al., 2012; Gallois, 2007), they have long been recognised to be  
61 a source of devastating volcanic hazards (e.g. Gudmundsson et al., 2008; Hansell and Oppenheimer,  
62 2004). Within active hydrothermal systems, the porous and fracture networks of the reservoir rocks  
63 may store high-pressure and temperature fluids that can be extracted for geothermal energy production  
64 (Gudmundsson, 1995) – a procedure established in 1904 by Italian scientist Piero Ginori Conti (Tiwari  
65 and Ghosal, 2005), and increasingly practiced in our efforts to deliver clean, renewable energy. The  
66 storage capacity of a reservoir is directly related to the porosity of the rock and the compressibility of  
67 the fluids (dependent on their chemistry), and our ability to extract these fluids requires a high degree  
68 of pore connectivity (e.g. Siratovich et al., 2014). Hence, permeability within exploited geothermal  
69 fields has an important control on both productivity and the sustainability of fluid flow within the  
70 reservoir. The development of permeability (whether natural or anthropogenic) has a great impact on  
71 the success, magnitude, and sustainability of energy production (Mock et al., 1997; Zimmermann et  
72 al., 2009).

73

74 The architecture of the porous network of rocks and, as a result permeability, varies widely in nature  
75 (e.g. Ashwell et al., 2015; Brace, 1980; Eichelberger et al., 1986; Farquharson et al., 2015; Heap et al.,  
76 2014a; Heap and Kennedy, 2016; Heap et al., 2014b; Heap et al., 2016; Jouniaux et al., 2000;  
77 Kendrick et al., 2016; Kendrick et al., 2013; Klug and Cashman, 1996; Kushnir et al., 2016; Lamur et  
78 al., 2017; Mueller et al., 2005; Okumura and Sasaki, 2014; Saar and Manga, 1999; Schaefer et al.,  
79 2015; Stimac et al., 2004). This is especially the case for volcanic rocks, as they have undergone  
80 complex petrogenetic and deformation histories during their formation (Farquharson et al., 2015;  
81 Kendrick et al., 2013; Klug and Cashman, 1996; Schaefer et al., 2015). For instance, during  
82 explosions, the pores which store the gas that triggers fragmentation are frozen into the lavas as they  
83 erupt; in contrast, the pore geometry of effusive lavas reflect a complex history of deformation, which

84 results from bubble growth, coalescence, collapse and fracturing. Dense volcanic rocks are generally  
85 found to contain flattened and/ or irregular (concave) pores and multiple micro-fractures, whereas  
86 highly vesicular volcanic rocks tend to have sub-rounded (convex) pores. As a result, explosive  
87 products have been described to hold a different permeability-porosity relationship than effusive  
88 products (Mueller et al., 2005). In addition, it has been suggested that there is a porosity change point  
89 (14~20 %) in microstructural control on effusive volcanic rock permeability, due to changes in relative  
90 tortuosity and pore throat size of the variably constructed porous networks of dense and porous rocks  
91 (Farquharson et al., 2015).

92

93 At depth, volcanic rocks may have different properties. Volcanic rocks buried by subsequent eruptive  
94 products – as is commonly the case in caldera systems (the setting of the geothermal system in this  
95 study) – tend to compact, closing micro-fractures (Kolzenburg et al., 2012), and if stress is sufficient,  
96 deformation may modify the architecture of the porous network (e.g. Heap et al., 2015a). Both micro-  
97 fracture closure (e.g. Lamur et al., 2017; Tanikawa and Shimamoto, 2009) and shear-enhanced  
98 compaction (Heap et al., 2015a) generally decrease the permeability of rocks buried at depth. When  
99 directly emplaced in the crust, intrusive volcanics tend to have low contents of vesicles and micro-  
100 fractures, and their permeability is equally low (Murphy et al., 1981), at least, at a small scale (Brace  
101 et al., 1968); yet, at a large scale, cooling contraction can trigger the development of columnar joints  
102 (Degraff and Aydin, 1993; Kantha, 1981), providing preferential fluid pathways.

103

104 Geothermal exploitation relies heavily on the presence of fractures to optimise fluid flow and energy  
105 generation. During drilling operations, a number of methods have been applied to enhance the extent  
106 of permeable fractures (e.g. Aqiu and Zarrouk, 2011), whether through hydraulic fracturing (e.g.  
107 Legarth et al., 2005; McClure and Horne, 2014; Miller, 2015; Murphy et al., 1981; Tomac and  
108 Gutierrez, 2017; Zang et al., 2014; Zimmermann et al., 2011) or thermal stimulation (e.g. Grant et al.,  
109 2013; Siratovich et al., 2015b). In high-temperature, high-enthalpy geothermal reservoirs, where the  
110 rock may exhibit ductile behaviour (e.g. Violay et al., 2012), it is commonly presumed that fractures  
111 would not remain opened nor preferentially oriented for long periods of time (e.g. Scott et al., 2015).

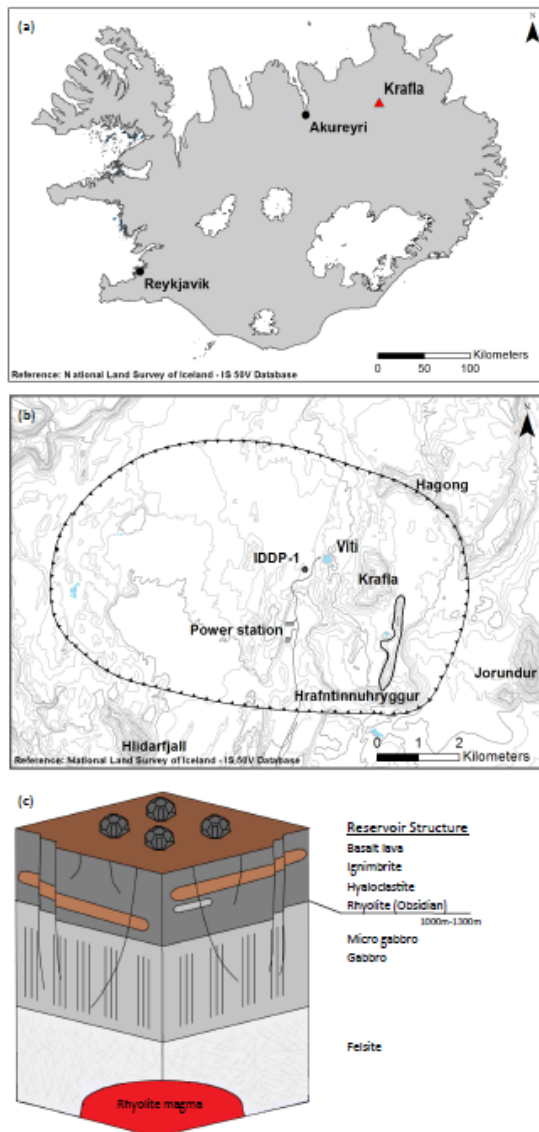
138 This may be the case if temperature is sufficient, such that the diffusivity of the main rock forming  
139 minerals and melt (if present), favours fracture healing (e.g. Farquharson et al., 2017; Lamur et al., In  
140 review; Tuffen et al., 2003) or viscous deformation of the porous network (Kendrick et al., 2013;  
141 Kushnir et al., 2017). However, such rapid closure of permeability can be overcome if the rock  
142 remains fractured by keeping stress sufficiently high (e.g. Lavallée et al., 2013), by building pore  
143 overpressure (e.g. Pearson, 1981) or by keeping temperature low (Lavallée et al., 2008), thus thermally  
144 contracting the rock (e.g. Siratovich et al., 2015b). Understanding the permeability of reservoir rocks,  
145 the sustainability of conditions and the longevity of production is key to characterising the potential  
146 exploitability of hydrothermal reservoirs for geothermal energy. Laboratory experimentation can help  
147 provide necessary constraints for material behaviour in simulated geothermal reservoir conditions  
148 (Ghassemi, 2012). For example, the presence of macroscopic fractures may significantly increase the  
149 permeability of rocks, especially of dense rocks (Eggertsson et al., 2016; Heap and Kennedy, 2016;  
150 Heap et al., 2015b; Lamur et al., 2017; Nara et al., 2012).

151

## 152 **1.2 Geological setting of the Krafla geothermal system**

153 Krafla is a caldera volcano, located in North-East Iceland (Figure 1a). The volcanic field hosts a partly  
154 filled caldera of about 8 x 10 km (Sæmundsson, 1991; [Figure 1b](#)) and is intersected by a 90 km long  
155 fissure swarm trending NNE (Hjartardottir et al., 2012). The caldera hosts an active hydrothermal  
156 system, approximately 10 km<sup>2</sup> in size. In the Holocene, fissure eruptions recurring every 300-1000  
157 years characterised the volcanic activity (Sæmundsson, 1991). In 1724, the Myvatn fires occurred west  
158 of Krafla; this coincided with a 5-year explosive phreatomagmatic eruption at Viti, which exposed at  
159 the surface gabbroic and felsitic lithics originating at depth in the system. The most recent eruption  
160 was the Krafla fires, which initiated in 1975 and resulted in the outpouring of basaltic lava for 9 years  
161 (Einarsson, 1991). Magmatic activity associated with the eruption impacted the chemical composition  
162 of the fluids within the reservoir (Guðmundsson, 2001; Ármannsson, 1989) and led to increased  
163 hydrothermal activity (Einarsson, 1978; Einarsson, 1991; Sæmundsson, 1991).

Deleted:



165  
 166 Figure 1: (a) Location of the Krafla volcanic field in North-East Iceland. (b) Overview of the Krafla  
 167 caldera, delimited by the line with tic marks (after Sæmundsson, 1991). The map shows the location of  
 168 key features, in particular the power station, the Viti crater, the drill site of IDDP-1 and  
 169 Hrafninnuhryggur (a large obsidian ridge). (c) Schematic of the lithologies comprising the Krafla  
 170 geothermal reservoir. The uppermost 1000 - 1300 m of the reservoir are primarily made up of  
 171 extrusive rocks, including lavas, ignimbrite and hyaloclastite. At greater depth, the reservoir is  
 172 dominated by intrusive volcanics, gabbro and felsite (Mortensen et al., 2015). In a part of the system,  
 173 rhyolitic magma was encountered at a depth of 2.1 km (Elders et al., 2014).

174  
 175 In 1974, the government of Iceland initiated the construction of a geothermal power plant within the  
 176 caldera. The aim was to install two turbines to produce 60MW<sub>e</sub>, but due to problems associated with  
 177 the Krafla fires eruption, the power plant only used one turbine until 1999; now that both turbines  
 178 operate, the power plant readily produces 60 MW<sub>e</sub> (Guðmundsson, 2001). In 2009 the Krafla

179 geothermal field became site of the Iceland deep drilling project (IDDP-1), with the aim to source  
180 deep, high-enthalpy, supercritical geothermal fluids at a depth of 4-5 km (Fridleifsson et al., 2014).  
181 This attempt terminated abruptly as the drill string penetrated an active rhyolitic magma body at a  
182 depth of 2.1 km (Elders et al., 2014). During flow tests of this, the World's hottest producing  
183 geothermal well, near-magmatic fluid entering the well head at a temperature exceeding 450 °C  
184 resulted in the transport of dry superheated steam at high pressures (40–140 bar), which due to its  
185 corrosive nature severely damaged the equipment and production ceased soon thereafter (Elders et al.,  
186 2014). Yet, this unique opportunity demonstrated the possibility of producing 35 MWe from a single  
187 well (Ingason et al., 2014), and helped define parts of the geothermal system for the first time,  
188 constraining the pressure (Elders et al., 2011) and temperature (Axelsson et al., 2014; Elders et al.,  
189 2011) conditions in the encountered rhyolite body. Volatile concentrations measured in glass shards  
190 recovered during drilling in magma were used to define a pressure of ~30-50 MPa (Zierenberg et al.,  
191 2013), which is lower than that expected from lithostatic pressure (ca. 50-70 MPa; considering a depth  
192 of 2.1 km and assuming a range of rock densities between 2.5~3.3 kg.m<sup>-3</sup>), but above hydrostatic  
193 pressure (~21 MPa) for this depth (Elders et al., 2011). This pressure discrepancy suggests that fluid  
194 pressure at the encountered magma body may be affected by connectivity across the hydrothermal  
195 system (e.g. Fournier, 1999).

196

197 Examination of drilling products (cores and cuttings) has provided a view of the rocks and structures  
198 hosting the reservoir fluids in the Krafla geothermal system. The observations suggest that the upper  
199 1000-1300 m of the reservoir, where temperatures are ca. 100-300 °C, primarily consists of variably  
200 indurated and welded ignimbrite, intact as well as fractured basaltic lavas and variably compacted  
201 hyaloclastite. At depths below 1000-1300 m, where temperature may reach ca. 350 °C, the reservoir is  
202 made up of intrusive volcanics, primarily gabbro and felsite, which both show variable degrees of  
203 fracture damage (Bodvarsson et al., 1984; Mortensen et al., 2014; Sæmundsson, 1991). The last rock  
204 encountered before reaching the near aphyric magma body during IDDP-1 was a felsite sill (argued to  
205 be the crystallised, mushy, magmatic aureole) which totalled ~80 m in thickness (Mortensen et al.,  
206 2014). This magmatic aureole is characterised by a sharp temperature increase from ~400 to ~900 °C

207 (e.g., Mortensen et al., 2014; Axelsson et al., 2014; Elders et al., 2014). Thus, 40 years of extensive  
208 drilling operations in and around the Krafla caldera has provided us with invaluable information that  
209 helped reconstruct the reservoir rock (Figure 1c). This study aims to constrain the permeability of  
210 these rocks, and assess how different thermal and mechanical stimulation methods may improve fluid  
211 flow in the hydrothermal system, and ultimately inform decisions to improve geothermal productivity  
212 in high-enthalpy systems.

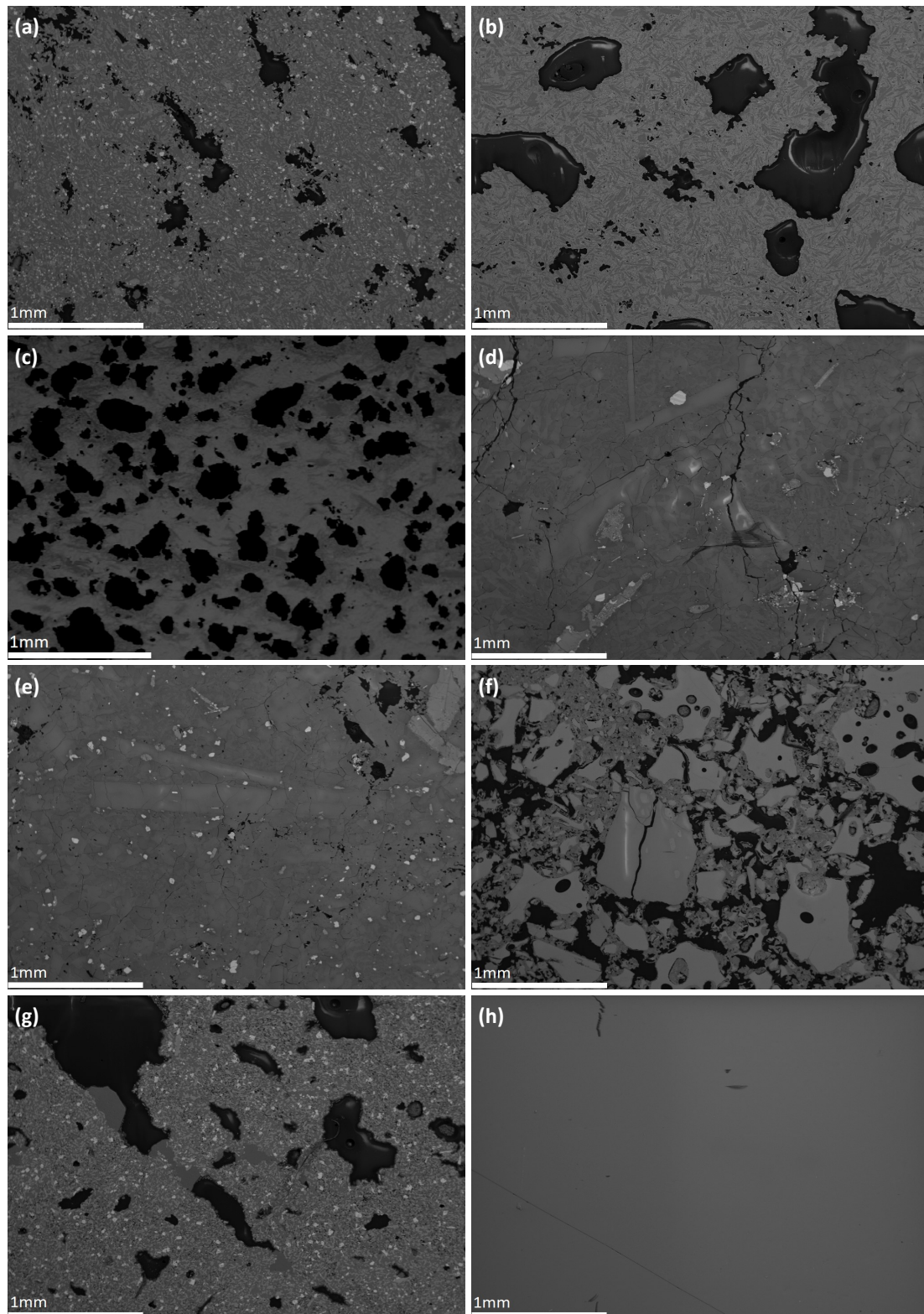
213

## 214 **2 Materials and Methods**

### 215 **2.1 Rock samples**

216 During a field survey in Autumn 2015, and through information gathered from previous drilling  
217 exercises, six main rock types were identified and sampled to carry out this study (see Supplementary  
218 Data): three basalts (a lava with 11 to 27 % porosity, a basalt dyke with 31-36% porosity, and a porous  
219 lava with 34 to 60 % porosity); one hyaloclastite (35-45 % porosity); one obsidian (1-5 % porosity);  
220 one ignimbrite (14-17 % porosity); one felsite (9-18% porosity) and one gabbro (11-15 % porosity).  
221 The samples host a spectrum of pore micro-structures (Figure 2), which we anticipated would result in  
222 equally diverse permeability properties. The samples were loose blocks (therefore not orientated),  
223 collected from surface outcrops without hammering to prevent adding fracture damage and  
224 compromising the porosity and permeability values determined here; the felsite and microgabbros  
225 (which form the roof of the magma reservoir; Mortensen et al., 2014) were erupted explosively  
226 through, and scattered around, Víti crater during the Mývatn fires (Sæmundsson, 1991).





227

228 Figure 2: Backscattered electron (BSE) images (obtained by scanning electron microscope (SEM)) of  
229 the main Krafla reservoir lithologies. (a) Microcrystalline basalt with 11 % porosity, consisting of  
230 irregular vesicles with a range of sizes ( $< 1$  mm), tortuosity and connectivity; micro-fractures are  
231 sparsely present but too narrow to be visible at this scale. (b) Microcrystalline basalt with 45 %  
232 porosity, comprising a bimodal porous network made of large and generally rounded, though slightly  
233 irregular, vesicles ( $< 2$  mm) and small irregularly-distributed vesicles; micro-fractures are sparsely

234 present but too narrow to be visible at this scale. (c) Basalt dyke sample with 32 % porosity,  
235 predominantly made of relatively evenly-distributed, sub-rounded vesicles (100-400 microns); the  
236 rock contains a trivial amount of very narrow micro-fractures. (d) Felsite with 11.5 % porosity,  
237 consisting of very few small and irregular vesicles, sometimes connected by micro-fractures, up to 10-  
238 20 $\mu$ m wide. (e) Gabbro with 12 % porosity, made up of a connected network of many small, irregular-  
239 shape vesicles, and poorly-developed micro-fractures. (f) Hyaloclastite with 40 % porosity, made up  
240 of irregular-shape pores between a highly fragmental, angular glass and crystalline assemblage. Micro-  
241 fractures as wide as 20  $\mu$ m are visible in larger fragments. (g) Ignimbrite with 15 % porosity,  
242 comprising generally elongate and sub-rounded vesicles, and a lack of micro-fractures visible at any  
243 scale. (h) Dense obsidian with scarce micro-vesicles (<0.01 %) and no obvious micro-fractures.

244

## 245 **2.2 Experimental methods**

246 Here, we aim to constrain the natural range of permeability of reservoir rocks and investigate how to  
247 enhance fluid flow by testing the effects of thermal and mechanical stimulation methods; including the  
248 impact of pressure oscillations, thermal stressing and fracturing. This was done in several steps: first,  
249 we measured the porosity and permeability of all rock samples as collected; second, we subjected  
250 them to the thermal or mechanical stimulation methods (see below); and finally, we measured the  
251 permeability anew.

252

253 In this study over 120 core samples were prepared from large blocks of the aforementioned six rock  
254 types, and tested to constrain the range of porosity and permeability of each: As loose samples of  
255 blocks were collected from outcrops with no strong fabrics, cores were prepared in no particular  
256 orientation, yet parallel to one another within a given block. To examine the influence of a macro-  
257 fracture on the permeability of rocks core samples with a diameter of 26 mm and a thickness of ~13  
258 mm were prepared; to investigate the impact of pressure fluctuations on permeability, cylindrical  
259 samples of felsite with a diameter and thickness of 26 mm were tested; for the investigation of thermal  
260 stressing impact on permeability, cylindrical samples of felsite and basalt with diameter of 25 mm and  
261 length of 50 mm were prepared and tested. The samples were kept in a drying oven at 75 °C after  
262 preparation, then left to cool in a desiccator before determinations of the porosity and permeability.  
263 The permeability dataset, obtained through the above experimental program, was complemented by  
264 additional porosity/ permeability measurements on 50 mm long by 25 mm diameter core samples (see

265 Supplementary Data), which will be used in a future mechanical study of Krafla rocks (Eggertsson et  
266 al., in preparation).

267

### 268 2.2.1 Porosity and Permeability

269 The connected porosity of the cores was determined using an AccuPyc 1340 Helium pycnometer from  
270 Micromeritics. The device measures the sample skeletal volume (i.e., the volume of the solid rock as  
271 well as isolated pores which cannot be accessed by helium gas) in chambers of 100 cm<sup>3</sup> and 35 cm<sup>3</sup>  
272 (depending on the size of the sample), which provides a volume determination accuracy for the sample  
273 of ±0.1 %. The measurement, together with the sample weight, constrains the relative sample density  
274 (including isolated pore space), and as we know the volume of the initial sample core, we can  
275 determine the fraction of connected pores.

276

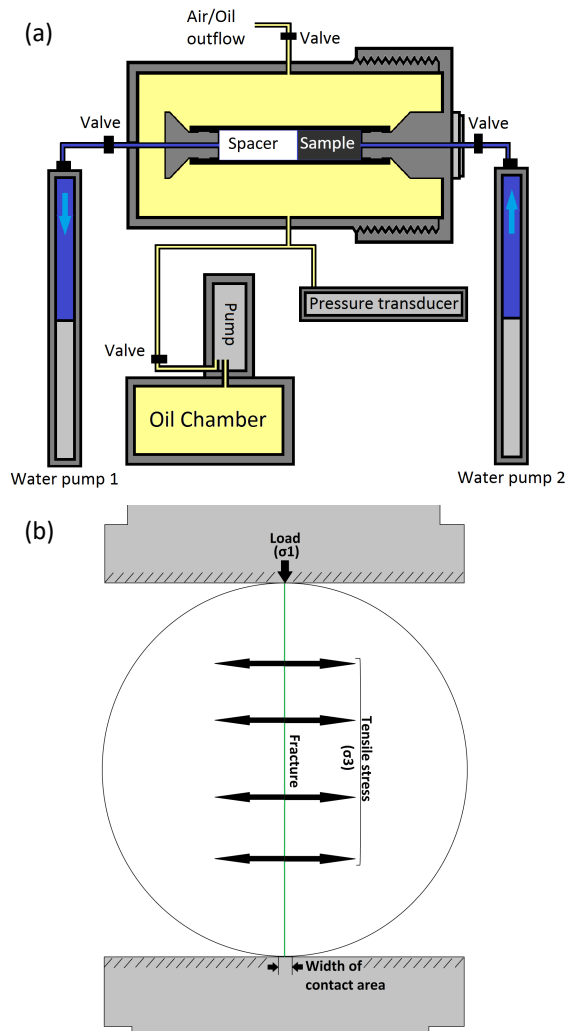
277 The permeability of the cores was measured in a hydrostatic pressure cell from Sanchez Technologies  
278 (Figure 3a) using the steady-state flow method. A water-saturated core was placed inside a rubber  
279 jacket and loaded in the pressure vessel, making sure that the pore pressure line was water saturated.

280 The sample assembly was then slowly pressurised using silicon oil to the desired confining pressures  
281 (5-100 MPa), spanning the conditions of the Krafla geothermal reservoir. As the sample was  
282 pressurised, the volume of water displaced by the sample compaction was monitored with a  
283 volumometer to track changes in the porosity (from the original porosity, measured by He-  
284 pycnometry) of the sample at various confining pressure. [The accuracy of the volumometer on the  
285 two Stigma 300 pumps (from Sanchez Technologies; now Core Lab) is 0.002 ml, which, when  
286 measuring fluid volume for the smallest sample volume of 6.9 cm<sup>3</sup>, results in an accuracy of porosity  
287 determination of 0.05 %.] Once equilibrated at the first confining pressure increment (e.g., 5 MPa) the  
288 rock permeability was measured using water, by imposing a pore pressure gradient of 1.5 MPa across  
289 the sample (2 MPa upstream and 0.5 MPa downstream) at an average pore pressure of 1.25 MPa, and  
290 by monitoring the flow rate at the sample exit; the permeability was only determined when the flow  
291 rate had stabilised. To assess the need for the use of Klinkenberg or Forchheimer corrections, the flow  
292 rate was varied by changing the pressure gradient and to check whether obtained permeability values

293 changed; for the pressure gradient of interest, no such corrections were needed here. Once the  
294 permeability measurement was completed (after 20 to 600 minutes), the confining pressure was  
295 increased to the next increment (e.g., 10 MPa), whilst monitoring pore volume changes [generally, the  
296 pore volume decrease would stabilise (within resolution of the volumometer) after 1-10 min]; then the  
297 permeability was measured anew.

298

299 To further constrain the elastic limits of the weak, porous hyaloclastite, we constrained the effective  
300 pressure threshold for inelastic, destructive compaction (defined as  $P^*$  of the rock), beyond which, an  
301 accelerated, irrecoverable compaction occurs (Zhang et al., 1990). This was done by loading a water-  
302 saturated sample in the permeameter. The confining pressure and pore pressure were increased slowly  
303 (to keep the effective pressure below 5 MPa) to 53 and 50 MPa, respectively. Then, the pore pressure  
304 was reduced (and thus the effective pressure was increased) at a rate of  $0.1 \text{ MPa}\cdot\text{min}^{-1}$  and the volume  
305 of water within the sample was monitored.  $P^*$  was defined as point of negative inflection following a  
306 linear decrease in pore volume during effective pressure loading.



307

308 Figure 3: (a) Schematic of the setup (hydrostatic cell and pumps) used to determine the permeability of  
 309 rocks. The permeability was measured using water (blue) by imposing a pressure gradient of 1.5 MPa  
 310 across the sample at an average pore pressure of 1.25 MPa (upstream: 2 MPa; downstream: 0.5 MPa)  
 311 for a range of confining pressures (5-100 MPa) exerted by silicon oil (in yellow). (b) Illustration of the  
 312 sample assembly to determine the tensile strength using the indirect Brazilian testing method. Here, a  
 313 disc of 2:1 ratio (26 mm diameter by 13 mm thickness) is diametrically loaded at a constant  
 314 displacement rate of  $3 \mu\text{m}\cdot\text{s}^{-1}$  between the pistons of an Instron press, and the load is continuously  
 315 recorded.

316

317

### 318 2.2.2 Pressure fluctuations

319 We tested the effects of pore pressure fluctuations over 10 cycles, whilst keeping the confining  
 320 pressure constant to simulate the impact of well pressure fluctuations associated with water injection  
 321 during drilling operations. This was performed on felsite samples which we loaded to 39.5 MPa

322 confining pressure and 1.5 MPa pore pressure (= 38 MPa effective pressure, assuming a simple  
323 effective pressure law). An effective pressure of 38 MPa may be representative of conditions at ca. 2  
324 km depth, near the hydrothermal-magmatic system interface (Mortensen et al., 2015). We then  
325 measured the permeability at these conditions by imposing a pressure gradient of 1 MPa across the  
326 sample (2 MPa upstream and 1 MPa downstream). Once the permeability was measured, the pore  
327 pressure was increased to 3.5 MPa and the permeability was measured by applying a pressure gradient  
328 of 1 MPa (4 MPa upstream and 3 MPa downstream). When the permeability had been measured at the  
329 lower effective pressure (higher pore pressure), the pore pressure was lowered back down to 1.5 MPa  
330 and the same procedure repeated, in total 9 times. The effective pressure change between each stage  
331 was therefore 1.5 MPa (from 38 MPa to 36.5 MPa effective pressure and back).

332

### 333 **2.2.3 Thermal stimulation**

334 The impact of thermal stimulation was tested on the samples of basalt (10.9-12.1 % porosity) and  
335 felsite (9.4-10.3 % porosity). The porosity and permeability of 3 cores of each sample was first  
336 measured as discussed above. The samples were then heated to 450 °C at 5°C/min in a box furnace  
337 and left for 1 hour to dwell. After that, one sample of each rock type was cooled in a furnace, with a  
338 set cooling rate of 5 °C.min<sup>-1</sup>; one sample of each rock was removed from the furnace and left to cool  
339 at ambient conditions on a benchtop; and finally, one sample of each rock type was removed from the  
340 furnace and quenched in a water-filled bucket at ambient temperature. Once cooled (estimated to be  
341 sufficient to cool the whole sample after 30 min – 12 hours, depending on the cooling method), the  
342 samples were then dried and their porosity and permeability were measured again. This procedure was  
343 repeated and the porosity and permeability were measured again after five and fifteen cycles. The  
344 cooling rates were chosen to represent different cooling rates experienced at different distances from  
345 boreholes during drilling activities and thermal stimulation procedures.

346

### 347 **2.2.4 Fracturing**

348 To induce a radial macro-fracture through the samples, the Brazilian tensile testing method was  
349 employed (Figure 3b). A cylindrical sample was loaded diametrically in a 5969 Instron uniaxial press

350 at a displacement rate of  $3 \mu\text{m}\cdot\text{s}^{-1}$  until a through-going fracture was produced. To ensure that the  
351 samples would not disintegrate during indirect tensile fracturing, the samples were carefully wrapped  
352 in electrical tape around the circumference (thus the mechanical data are not of publishable quality).  
353 After sample failure, the tape was carefully removed and the sample loaded into the pressure vessel for  
354 another series of permeability determinations.

355

356 For six basalt samples, a second set of fractures was then imparted, perpendicular to the first fracture  
357 in the samples. This time, however, the sample was left in the rubber jacket during loading in the press  
358 to ensure coherence. After sample failure, the permeability was measured once again under the same  
359 range of conditions as detailed above.

360

361

## 362 **3 Results**

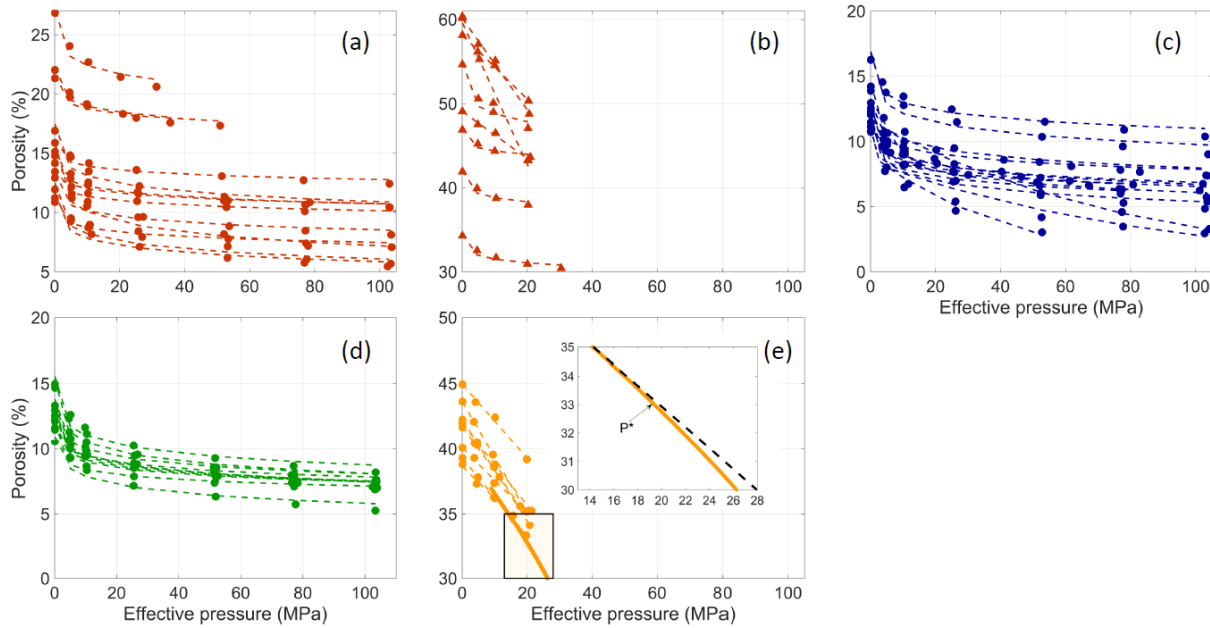
### 363 **3.1 Storage capacity of intact rocks**

364 The porosity of a rock is a measure of the storage capacity for fluids and varies as a function of  
365 effective pressure (Wong and Baud, 2012). Here, we combine He-pycnometry measurements at  
366 atmospheric pressure (i.e., effective pressure of 0 MPa) and fluid volume changes measured by the  
367 volumometer in each pump during pressurisation and depressurisation in the hydrostatic pressure  
368 vessel, to constrain the evolution of porosity upon confinement.

369

370 The lithologies tested exhibit a wide range of porosities; especially the three basalt samples, which  
371 contain between 11 and 60 vol. % porosity. The porosity evolution as a function of effective pressure  
372 could only be measured for four rock types (Figure 4), as the obsidian and the ignimbrite had  
373 permeabilities too low to be determined using our setup in its current configuration (which cannot  
374 accurately constrain permeability lower than  $\sim 10^{-18} \text{ m}^2$ ). In all cases, the samples show a nonlinear  
375 decrease in pore volume with effective pressure. We note that the spread of porosity within each  
376 sample set is not particularly sensitive to effective pressure, suggesting that the nonlinear decrease in  
377 porosity with effective pressure is similar for a given rock type. For the most porous samples, the

378 porosity decrease is slightly more pronounced (Figure 4b,e), which may be accentuated if the effective  
 379 pressure exceeds  $P^*$ , resulting in crushing of the rock and compaction (e.g., hyaloclastite; inset Figure  
 380 4e).  
 381



382  
 383 Figure 4: Porosity evolution with effective pressure for intact (a) dense basalt (shown in Figure 2a; 10  
 384 samples tested), (b) porous basalt (shown in Figure 2b; 6 samples), (c) felsite (14 samples), (d) gabbro  
 385 (10 samples), and (e) hyaloclastite (8 samples) as a function of effective pressure. Here, the initial  
 386 porosity measurement is made by He-pycnometry, with subsequent measurements extrapolated by  
 387 monitoring volume gain in the pumps (hence volume loss in the samples) during permeability  
 388 measurements. The figure shows a nonlinear decrease in porosity with effective pressure, indicative of  
 389 micro-fracture closure. Across the lithologies, porosity decreases most rapidly as effective pressure is  
 390 increased up to  $\sim 10$  MPa. Note that the scale of each graph differs. The inset in (e) shows the inelastic  
 391 (destructive) compaction beyond  $P^*$ , where the rock strength is not sufficient to withstand the increased  
 392 pressure and starts to collapse.

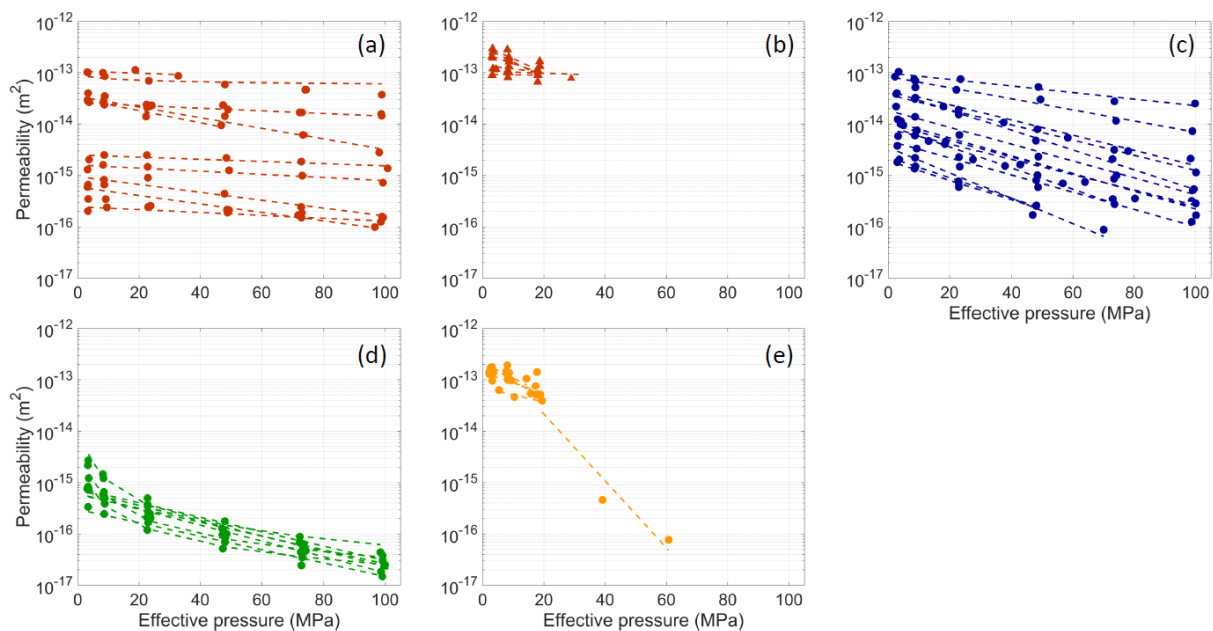
393

### 394 3.2 Permeability of intact rocks

395 The permeability of rocks varies as a function of porosity (e.g., Mueller et al., 2005), fracture density  
 396 (e.g. Heap and Kennedy, 2016; Koudina et al., 1998) and effective pressure (e.g. Alam et al., 2014;  
 397 Walsh, 1981). Here, we present permeability measurements on 60 intact samples; the basalt ( $1.9 \times 10^{-16}$   
 398  $\text{m}^2 - 2.5 \times 10^{-13} \text{ m}^2$ ), felsite ( $1.8 \times 10^{-15} \text{ m}^2 - 1.1 \times 10^{-13} \text{ m}^2$ ), gabbro ( $7.2 \times 10^{-16} \text{ m}^2 - 1.0 \times 10^{-14} \text{ m}^2$ ) and  
 399 hyaloclastite ( $6.0 \times 10^{-14} \text{ m}^2 - 1.8 \times 10^{-13} \text{ m}^2$ ) samples show a range of permeabilities (Figure 5). The data



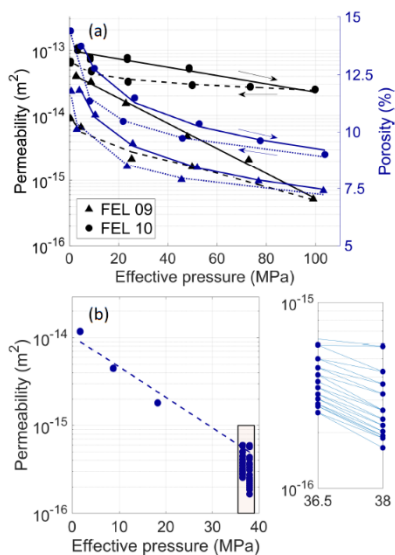
400 show that sample length (used here) has no effect on the permeability of a rock (see Supplementary  
 401 Data). The basalts displayed the widest range of permeabilities (Figure 5: 5a, b), as might be expected  
 402 from their variable initial porosities (Figures 2a-c, 4a, b). [Note that the basalt dyke was not measured  
 403 under such conditions.] The densest basalt shows little change in permeability with increased pressure  
 404 (Figure 5a). The basalt samples with the highest porosities (>34 vol. % porosity; Figure 5b) show a  
 405 small decrease of permeability with confining pressure (up to 20-25 MPa); lower than may be  
 406 anticipated due to the porosity decrease witnessed upon pressurisation (Figure 4b). The felsite and  
 407 gabbro samples exhibit relatively larger decreases in permeability (Figure 5c,d) in response to  
 408 effective pressure than the basalts (Figure 5a), owing to the highly fractured nature of these rocks. Yet,  
 409 despite a fragmental origin of the hyaloclastite (Figure 5e), it only exhibited moderate decrease in  
 410 permeability within the low effective pressure range tested (before the samples could not sustain the  
 411 effective pressure); however, the samples compacted inelastically above an effective pressure of 18  
 412 MPa (inset Figure 4e), which resulted in a significantly lower permeability.



413  
 414 Figure 5: Intact rock permeability evolution with effective pressure of (a) dense basalt (10 samples  
 415 tested), (b) porous basalt (6 samples), (c) felsite (14 samples tested), (d) gabbro (10 samples tested),  
 416 and (e) hyaloclastite (8 samples tested). The general nonlinear decrease in permeability with effective  
 417 pressure is attributed to the compaction and closure of micro-fractures as observed by the porosity  
 418 volume decrease in Figure 4.  
 419

### 420 3.3 Impact of pressure fluctuations

421 During a well operation, changes in pore pressure are inevitable, from injection during drilling to  
422 functional operation at different pressures. These changes can be considered minor, but their resulting  
423 influence on the rock permeability remains poorly tested. Here, we investigate the impact on the  
424 permeability of pressurising and depressurising highly fractured felsite samples. When decreasing the  
425 pore pressure applied to a sample (at a set confinement), we note a slight increase in the rock porosity  
426 and permeability (Figure 6a); yet, not as significant as the magnitude of porosity and permeability  
427 decrease monitored during pressurisation. Thus, pressurisation and depressurisation of porous rocks



428 leads to hysteresis of its permeable structure on the timescales investigated here.

429

430 Figure 6: Variations of: (a) Permeability and porosity of felsite resulting from pore pressure (and thus  
431 effective pressure) loading/ unloading cycles to 100 MPa. The figure shows a degree of hysteresis; as  
432 effective pressure is decreased the sample does not recover the initial (i.e., lower pressure)  
433 permeability and porosity of the rock. (b) Permeability evolution of felsite during pore pressure  
434 (hence, effective pressure) oscillations of 1.5 MPa. The data (zoomed-in inset in b) shows that each  
435 unloading cycle never fully recovers permeability efficiency, and the permeability lowers further with  
436 each loading cycle due to further closure of permeable pathways.

437

438 The hysteresis of a rock porous structure to pressure fluctuations were investigated further by testing  
439 the impact of 10 pressurisation/ depressurisation cycles on the felsite by first pressurising the sample  
440 to the target confining pressure of 38 MPa (left for 30 min to equilibrate each time the pressure was

441 changed), and fluctuating the pore pressure by 1.5 MPa (Figure 6b). Interestingly, we note that each  
 442 pressurisation cycle decreases the permeability of the rocks, which never fully recover during  
 443 depressurisation (Figure 6b). The impact is most pronounced in the first few cycles, but persists  
 444 throughout all 10 cycles.

445

### 446 3.4 Impact of thermal stimulation

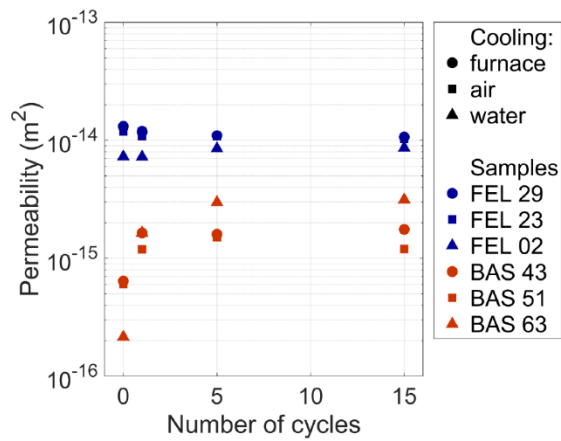
447

448 Table 1. Porosity of volcanic rocks subjected to thermal stressing cycles.

Number of cycles	Porosity (%)			
	0	1	5	15
FEL_TRI_29	10.3	10.5	10.3	10.5
FEL_TRI_23	9.4	9.3	9.4	9.3
FEL_PP_02	9.8	9.8	9.9	9.9
BAS_TRI_43	11.5	11.5	11.4	11.4
BAS_TRI_51	12.1	12.2	12.1	12.0
BAS_TRI_63	10.9	11.1	10.9	11.1

449

450 During well drilling and operation, the reservoir temperature fluctuates. To test the effect of  
 451 temperature changes, we subjected felsite and basalt to thermal stress cycles by cooling from 450 °C  
 452 to ambient temperature by cooling in a furnace (under controlled conditions), in air (on a benchtop) as  
 453 well as in water (at ambient temperature, to quench). The data shows that the porosity and  
 454 permeability of the felsite was not affected by thermal stressing, even after fifteen heating/cooling  
 455 cycles (Table 1; Figure 7). On the other hand, the porosity of the basalt was relatively unchanged  
 456 (Table 1), while the permeability of the basalt increased by over one order of magnitude after the first  
 457 five cycles; the most drastic impact being imposed by quenching in water (Figure 7).



458

459 Figure 7: Influence of thermal stressing (up to 450 °C) cycles on the permeability of basalt (BAS) and  
 460 felsite (FEL) cooled under different conditions. The data show that the permeability of the felsite is  
 461 insensitive to thermal fluctuations, presumably as the original sample contains multiple micro-  
 462 fractures (see Figure 2). In contrast, the permeability of the basalt non-linearly increases with thermal  
 463 cycles (especially the first five cycles). We note that permeability is highest in samples cooled by  
 464 water (triangles), compared to cooling in ambient air or under controlled conditions in the furnace  
 465 (i.e., at <5 °C.min<sup>-1</sup>).

466

### 467 3.5 Impact of one macro-fracture

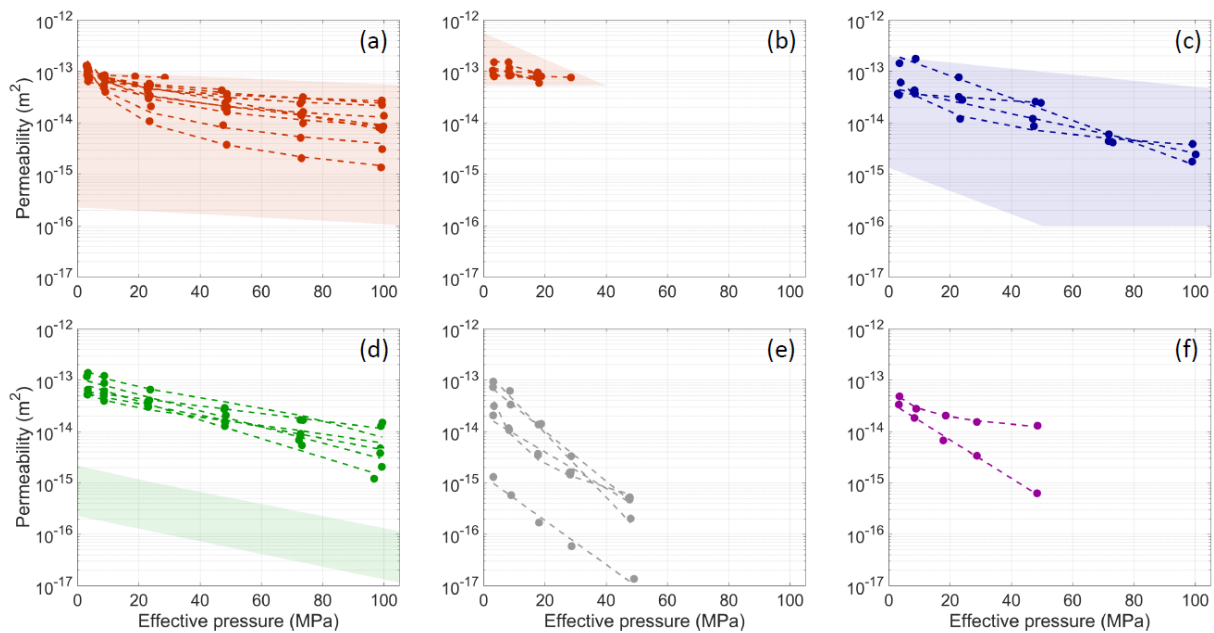
468 The effect of a macro-fracture on the permeability of a sample has been the focus of recent studies  
 469 (Heap and Kennedy, 2016; Lamur et al., 2017; Nara et al., 2011); here we expand this dataset by  
 470 testing the impact of macro-fractures on several lithologies. Of the lithologies tested here, the  
 471 hyaloclastite did not withstand a fracture, but rather compacted during Brazilian tensile testing, and  
 472 therefore the permeability of fractured hyaloclastite could not be measured. Similarly, of the felsite  
 473 cores tested, only a few developed clean fractures during mechanical testing, therefore reducing the  
 474 number of fractured samples measured for permeability. The basaltic dyke was not subjected to this  
 475 testing method (as we had insufficient material).

476

477 For the dense basalt and felsite, for which intact samples showed a wide range of permeabilities, the  
 478 presence of a fracture narrowed the range of permeabilities to relatively high values (Figure 8a, c). In  
 479 contrast, the permeability of the porous basalt was not affected by the addition of a macro-fracture  
 480 (Figure 8b). For all other samples, imparting a fracture increased permeability by as much as 2-5  
 481 orders of magnitude (Figure 8d-f).

482

483 Effective pressure showed variable influences on the permeability (Figure 5) of these macro-fractured  
484 rocks; yet, permeability decrease was generally greatest in the early stages of confinement, and for  
485 most samples led to a nonlinear decrease of 1-2 orders of magnitude of permeability (Figures 8 and 9).  
486 The sensitivity of permeability of fractured samples to confinement was heightened as compared to  
487 their intact counterparts (Figures 5 and 8). Within one lithology (basalt) however, the sensitivity to  
488 confinement was variable (Figure 9); yet, these macro-fractures are irregular, and bordered by minor  
489 fractures and fragments (Figure 10).



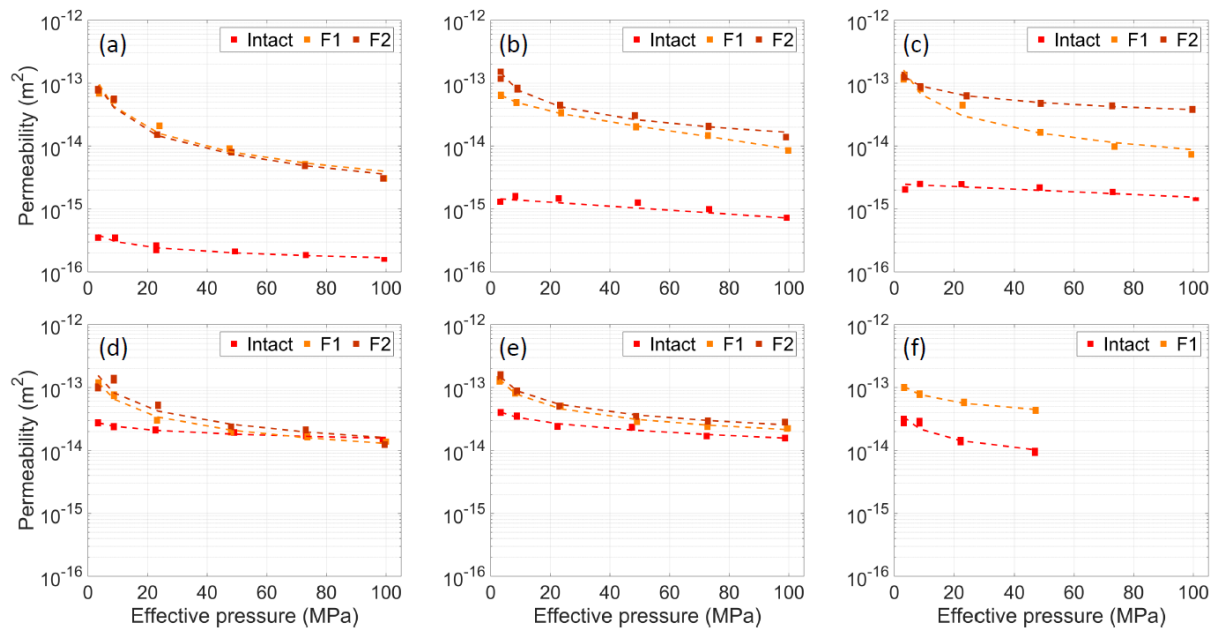
490

491 Figure 8: Permeability evolution with effective pressure of macro-fractured (a) dense basalt (10  
492 samples), (b) porous basalt (5 samples), (c) felsite (4 samples), (d) gabbro (6 samples tested), (e)  
493 Ignimbrite (5 samples), and (f) obsidian (2 samples). The shaded areas show the range of permeability  
494 of intact samples before they were fractured (from Figure 5: ), showing the variable effect of fractures  
495 on permeability. Note that the permeability of the intact ignimbrite and obsidian was below the  
496 detection limit for our apparatus (which was developed for permeable samples).

497

### 498 3.6 Impact of two macro-fractures

499 The basalts, being a key rock type in Iceland and the most mechanically consistent rock of the  
500 lithologies at Krafla, were used to test the impact of two orthogonal macro-fractures on the permeable  
501 porous network, as they display a wide range of initial porosities and permeabilities. The tests were  
502 systematically conducted on six samples, ranging between 10.9 and 21.3 vol. % porosity.



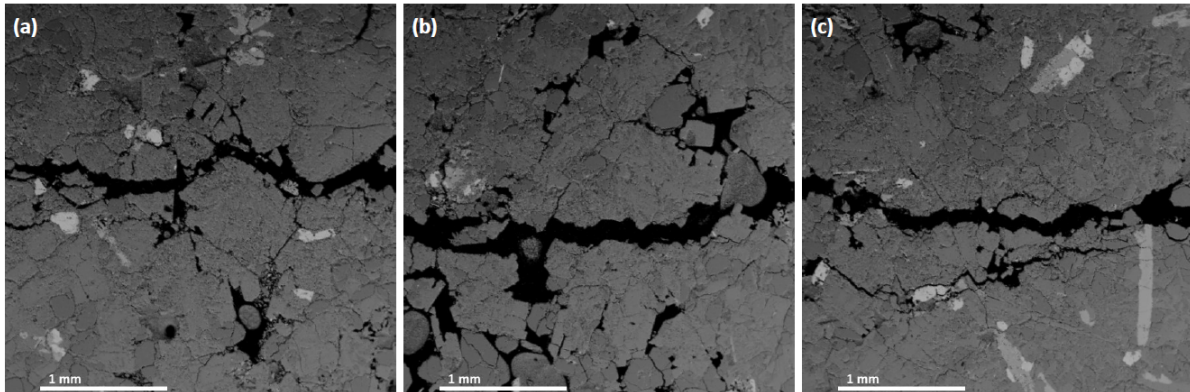
503  
 504 Figure 9: Permeability variations with effective pressure for intact samples, and the same samples with  
 505 one fracture (F1) and two fractures (F2), imparted experimentally for basalts with a range of initial  
 506 porosities from (a) 10.9 %, (b) 12.9 %, (c) 13.5 %, (d) 14.8 %, (e) 15.9 % to (f) 21.3 %. The data show  
 507 a 0.5 to >2 order of magnitude increase in permeability due to fracturing, which is more significant at  
 508 low porosity. Increasing effective pressure closes the fracture and the permeability nonlinearly  
 509 decreases, trending towards that of the intact rock. This convergence is not always possible,  
 510 presumably as in imperfect contact or dislodged fragments may obstruct fracture closure (See Figure  
 511 10).

512

513 The generation of a second, orthogonal fracture increased the permeability of the rocks further for  
 514 samples across the range of porosities tested. The most porous sample (Figure 9f) was unable to  
 515 sustain the fracture and crumbled. The permeability increase induced by the second fracture was not as  
 516 significant as the first fracture (Figures 8-9), despite creating more fracture surface area and increasing  
 517 porosity. This observation remains valid over the range of effective pressures tested; the interesting  
 518 exception to this is the sample with 13.5 % porosity, for which the second fracture seems not to close  
 519 adequately with an increase in effective pressure, resulting in a permeability nearly an order of  
 520 magnitude higher than the single-fractured sample at 100 MPa effective pressure. For all other  
 521 samples with 1 or 2 fractures, upon confinement, the permeability trends towards that of the intact  
 522 rock. This convergence is not always possible, and appears less readily attainable in the lower porosity  
 523 samples (Figure 9a-c), which have the lowest initial permeability values and for which the  
 524 permeability is most affected by fracturing.

525

526



527

528 Figure 10: Backscattered electron (BSE) images (obtained by scanning electron microscope (SEM)) of  
529 fractures generated in the felsite (average 11.5 % porosity). The images show that failure was  
530 accommodated by a macro-fracture, hosting small rock fragments and bordered by fine, branching  
531 subparallel fractures, with slight variability within one lithology.

532

#### 533 4 Discussion and implications

534 The findings presented here enhance our understanding of the impacts of thermal and mechanical  
535 stimulation practices. The data shows that pore pressure fluctuations at pressures lower than the local  
536 confining pressure may not be an effective way to increase the permeability of a reservoir; yet, we  
537 surmise that if this pore pressure variation takes place at pressures nearing or exceeding the local stress  
538 – a condition favouring tensile fracture propagation (see section 4.1), then the effect may be quite  
539 contrasting (e.g. Rozhko et al., 2007). Thermal stimulation demonstrated variable influence on the  
540 resultant permeable porous network. Here, we noted that rocks void of micro-fractures were more  
541 liable to thermal stressing than micro-fractured rocks. This may be because, when present in a rock,  
542 micro-fractures may simply open during cooling contraction of the solid phase, without building large  
543 tensile stresses; in contrast, crack-poor rocks would build up large tensile stresses during cooling  
544 contraction, which may result in cracking, and thus enhanced fluid flow. The observed change in  
545 permeability of about one order of magnitude is moderate compared to Siratovich et al. (2015a), which  
546 showed a permeability change by three orders of magnitude for the dense andesite of the Rotokawa  
547 geothermal field. Thus, the permeability of hydrothermal reservoirs may be subject to changes in the  
548 lifetime of fluid extraction if it results in temperature changes, especially if rapidly heating and cooling

549 dense unfractured lithologies. Yet ultimately, it is the generation of fractures, whether microscopic or  
550 macroscopic in nature, which controls permeability in the reservoirs, and arguably when fractures are  
551 mechanically impeded from adequate closure that they present the most persistent fluid pathways.

552

#### 553 **4.1 On the permeability of intact and fractured volcanic rocks**

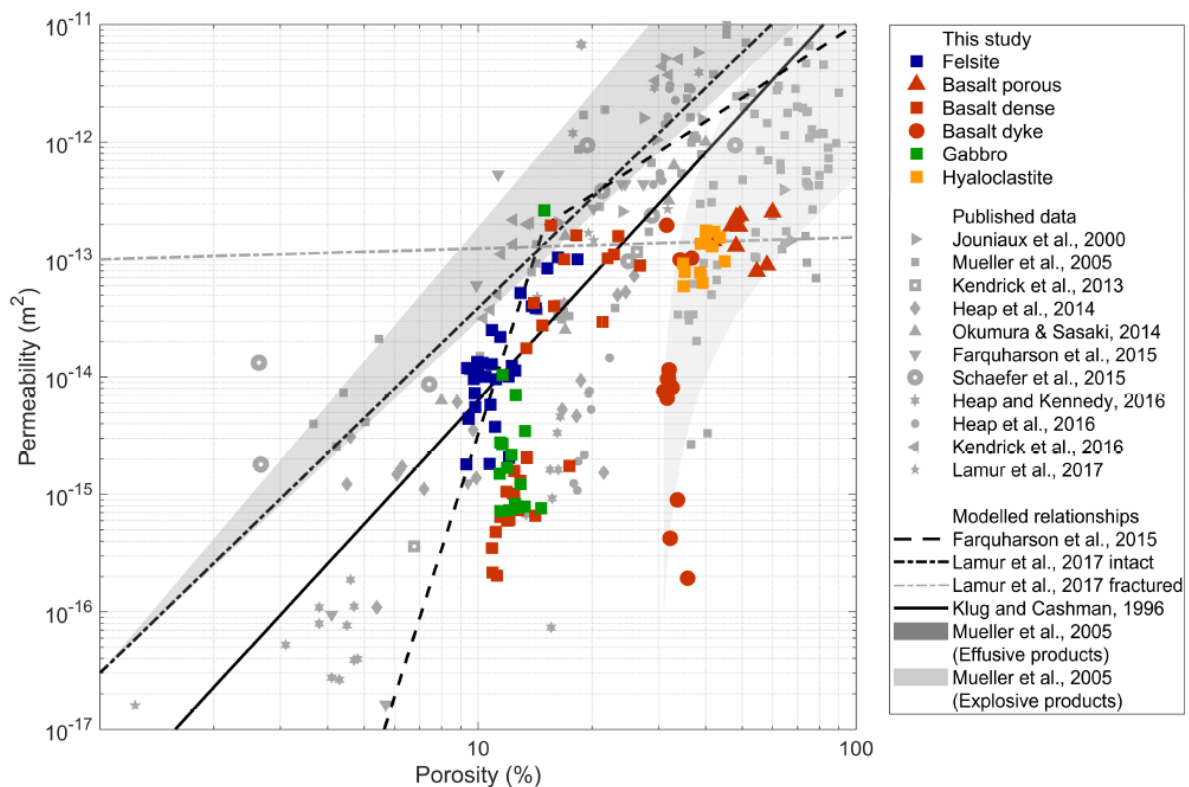
554 Detailed knowledge of the storage capacity and permeability of reservoir rocks is crucial to improve  
555 the utilisation of geothermal resources and to maximise energy production. The experimental work  
556 carried out here sheds light on the efficiency of fluid flow through the permeable porous network in  
557 the Krafla geothermal reservoir. The reservoir consists of a succession of mafic lavas, ignimbrites and  
558 hyaloclastites at shallow depth (<1 km) and at greater depth (>1 km), of cross-cutting mafic,  
559 intermediate and felsic intrusions (Mortensen et al., 2015). All the rocks display a range of porosities  
560 and permeabilities, and correspondingly, differing responses to effective pressure. The rocks found at  
561 shallow depths are highly variable: the basaltic rocks have a wide range of porosities and  
562 permeabilities, and the densest lithologies remain strong when pressurised (or, in natural terms,  
563 buried); whereas the porous basalt and hyaloclastite can only experience relatively low confinement  
564 without undergoing compaction (at  $P^*$ ). The intrusive rocks originating at depth were observed to be  
565 highly fractured, which led to high permeability (and higher dependence of permeability on effective  
566 pressure), despite their low porosities. The basaltic dyke however has low permeability, despite  
567 relatively high porosity (32-34 vol. % porosity; Figure 11), due to a predominantly isolated pore  
568 structure (Figure 2c). Within the reservoir, we expect that other dykes may be denser and less  
569 permeable.

570

571 When compiled together, the permeability of the intact rocks increases non-linearly with porosity  
572 (Figure 11), as previously described (e.g. Ashwell et al., 2015; Brace, 1980; Eichelberger et al., 1986;  
573 Farquharson et al., 2015; Heap et al., 2014a; Heap and Kennedy, 2016; Heap et al., 2014b; Heap et al.,  
574 2016; Jouniaux et al., 2000; Kendrick et al., 2016; Kendrick et al., 2013; Klug and Cashman, 1996;  
575 Kushnir et al., 2016; Lamur et al., 2017; Mueller et al., 2005; Okumura and Sasaki, 2014; Saar and  
576 Manga, 1999; Schaefer et al., 2015; Stimac et al., 2004). [It should be noted that previously published



577 data collected at slightly different effective pressures (e.g. Tanikawa and Shimamoto, 2009) may  
 578 increase scatter.] As permeability-porosity measurements of a variety of volcanic rocks accrue (e.g.  
 579 Farquharson et al., 2015; Lamur et al., 2017; Mueller et al., 2005), a picture is rapidly emerging which  
 580 depicts a wide range of permeabilities at all porosities (e.g., at ~10 % and ~35 % in Figure 11); here,  
 581 we advance that the absence of a petrogenetic link between rocks with different porosities and  
 582 permeabilities (owing to distinct petrological and deformational histories) may preclude the necessity  
 583 to invoke a change point dividing two permeability regimes – fracture- vs vesicle-controlled – (even if  
 584 statistically determined by the current dataset) and that a simple power-law regression may be an  
 585 equally adequate approximation to be used in simulations, until a genetic link is established.



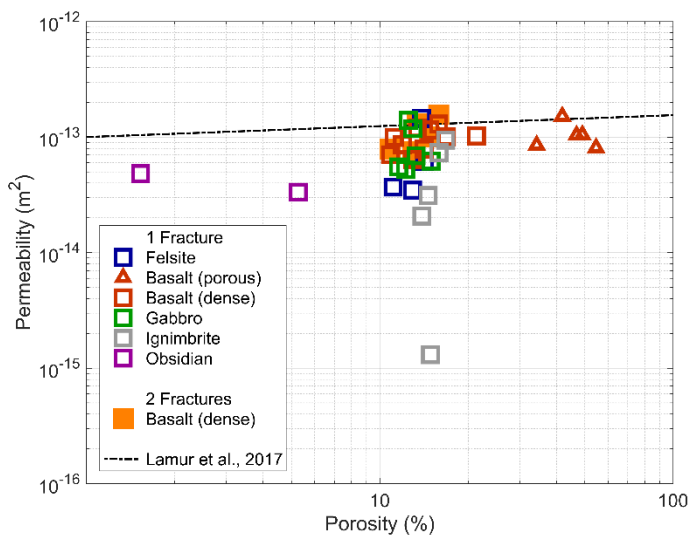
586

587 Figure 11: Permeability (measured at  $P_{\text{eff}}=3,75$  MPa) as a function of porosity, showing the extensive  
 588 variability of the lithologies examined. Data from this study correlate well with previously published  
 589 data (measured at a range of effective pressures, which increases scatter further). Comparing the data  
 590 to models to describe the porosity-permeability relationship, we note that the model for explosive  
 591 products from Mueller et al. (2005) correlates very well with samples collected from a dyke. For the  
 592 lower porosity samples, the model proposed by Farquharson et al., (2015) shows a better correlation  
 593 than other models proposed, with a rapid increase in permeability over relatively narrow range of  
 594 porosity, although above the inflection point the trend does not correlate well. Rather, it appears that

595 the relationship for fractured rocks from Lamur et al. (2017) appropriately describes the upper limit of  
596 permeability observed here.

597

598 The addition of a macro-fracture increases the permeability of porous volcanic rocks. Recent  
599 experimental investigations (Heap and Kennedy, 2016; Lamur et al., 2017) have proposed models to  
600 constrain the impact of fractures on permeability as a function of effective pressure, demonstrating  
601 that in the presence of one fracture, the permeability-porosity relationship follows a power law  
602 dependence (Lamur et al., 2017); here, our dataset appears to abide to such a power-law relationship  
603 (Figure 12). The permeability-porosity relationship of fractured volcanics further appears to limit the  
604 permeability of all porous rocks (>15 vol. % porosity) present at Krafla (Figure 11).



605

606 Figure 12: The connected porous network of the fractured samples shows a very narrow variability of  
607 permeability across all lithologies, typically less than 1 order of magnitude ( $P_{eff}=3.75$  MPa) across a  
608 wide range of starting porosities. The data is compared to the relationship for fractured rock  
609 permeability described in Lamur et al. (2017) for the correct effective pressure. This relationship  
610 appropriately to describe the dataset with both 1 and 2 macrofractures, as well as appearing to describe  
611 the upper permeability limit of our intact samples (Figure 11).

612

613 The data presented here further suggest that the obstruction of fractures by particles locally fragmented  
614 and offset between fracture planes may prevent complete fracture closure (Figure 10). This influence  
615 is more likely as more fractures are introduced, and results in persistence of high permeability even at  
616 high effective pressures. Perez-Flores et al. (2017) showed that the effect of fracture offset on

617 permeability varies between lithologies, but at a certain offset length, the effect on permeability  
618 reached a maximum, which for fresh basalt, was around two orders of magnitude of permeability.  
619 With time, offset fractures also withhold a better permeability, by keeping the fracture network open  
620 even if pressure changes (Hofmann et al., 2016), as we observe. Fracture closure and fracture network  
621 response to changes in effective pressure have also been shown to be controlled by the mechanical  
622 properties of a rocktype, as stronger rocks may prevent efficient fracture closure, whereas weak rocks  
623 may deform and shut fractures (Milsch et al., 2016). Slurries containing sand particles with the  
624 purpose of obstructing fracture closure have been used to optimise reservoir permeability and fluid  
625 extraction (Brinton et al., 2011), and our findings corroborate these practices. We further suggest that  
626 strategic thermo-mechanical stressing to impart fractures which orthogonally intersect local or  
627 regional fractures may be an equally efficient way to increase the permeability of a reservoir and thus,  
628 its resultant energy output. The outcome of this practice may likely be enhanced if the fracture  
629 produced is strategically aligned at low angles to the principal stress (in an anisotropic stress field) to  
630 favour slight displacement/ misalignment of the fracture interfaces, which may leave gaps in the rock  
631 to permit extensive fluid flow. This effect may be central to the efficiency of thermo-mechanically  
632 derived fractures as pathways to increase connectivity in the reservoir.

633

#### 634 **4.2 Permeability of the Krafla hydrothermal reservoir**

635 Today at Krafla, geothermal energy production focuses on fluid extraction at shallow depth up to  
636 about 2-3 km (Mortensen et al., 2015); yet, deeper fluid extraction is often contemplated in our pursuit  
637 of higher energy production (Fridleifsson et al., 2014). In doing so, efforts must be made to avoid  
638 intersecting the shallow magma reservoir located at a depth of 2.1 km (Elders et al., 2014).  
639 Geochemical investigation of the glass fragments recovered during drilling into the magma reservoir  
640 suggests that volatile concentration is in equilibrium with a temperature of 800-950 °C (Axelsson et  
641 al., 2014; Elders et al., 2011) and a pressure of 30-50 MPa (Elders et al., 2011). At Krafla, a depth of  
642 2.1 km corresponds to a lithostatic pressure of approximately 65 MPa, if we assume a rock density of  
643 3,100 kg/m<sup>3</sup> for the predominantly basaltic chemistry of these volcanics; thus, the discrepancy  
644 between the estimated equilibrium and the approximation of the lithostatic load suggests that fluid

645 connectivity in the hydrothermal system may be efficiently decrease local magmatic pressure to below  
646 lithostatic. Thus, we can assume that at any given depth in the Krafla hydrothermal reservoir, the  
647 effective pressure can be approximated by subtracting the hydrostatic pressure (i.e., the pore pressure  
648 in our experiments) from the lithostatic pressure (i.e., the confining pressure in our experiments).  
649 Therefore, a depth of 2-3 km may correspond to effective pressures of 40-50 MPa (in agreement with  
650 equilibrium conditions for the glass; Elders et al., 2011). The study shows that the storage capacity and  
651 permeability of the reservoir rocks nonlinearly increases by decreasing the effective pressure exerted  
652 in the system, so fluid extraction may be optimised by ensuring high pressure of fluid injected into the  
653 hydrothermal system to keep fractures open as wide as permits (whilst remaining stable and not  
654 creating undesired hydraulic fractures).

655  
656 During IDDP-1, drilling activities suffered from a loss in fluids shortly before intersecting the magma  
657 reservoir at 2.1 km (Palsson et al., 2014). This 50-m thick zone of fluid loss coincided with  
658 encountering felsite – a crystalline rock believed to represent the crystallised aureole that surrounds  
659 the magma reservoir (Mortensen et al., 2014). No large samples of felsite were retrieved by the  
660 drilling activities, but samples can be collected from the phreatomagmatic deposits that surround the  
661 Viti crater (Sæmundsson, 1991). In this study, we examined gabbro and felsite blocks from this  
662 phreatomagmatic event and we found that both samples are highly micro-fractured (Figure 2d, e),  
663 which results in high permeability (and fracture compressibility with effective pressure).  
664 Phreatomagmatic eruptions are known to be highly explosive (Austin-Erickson et al., 2008) and we  
665 postulate that the high fracture density observed in the samples tested here is congruent with their  
666 eruption and with a damaged source region. Deep-seated fragmentation at depths of ca. 2.1 km,  
667 perhaps even due to emplacement of the rhyolitic magma, may thus be at the origin of this felsitic  
668 zone with high-fracture density that led to important fluid loss during IDDP-1. If such is the case, the  
669 high permeability of fractured magmatic aureoles – commonly believed not to have open fractures due  
670 to their propensity to flow and heal (e.g. Scott et al., 2015) – may be key in ensuring fluid connectivity  
671 between the Earth's surface and the magma reservoir. This permeable architecture may naturally

672 prevent from the accumulation of excess volatile concentration, dissolved in the magma, making it not  
673 particularly buoyant and hence unlikely to erupt during drilling operations.

674

675 The laboratory measurements performed on samples primarily collected from surficial outcrops at  
676 Krafla, offer a first order constraint on the storage capacity and permeability of the reservoir rock  
677 present at Krafla volcano. Yet, much remains to be investigated to obtain a complete picture of fluid  
678 flow in this hydrothermal system: from complexity arising from the effects of high-temperatures  
679 (Kushnir et al., 2017) to the influence exerted by devolatilisation (e.g. Heap et al., 2013), dissolution  
680 (Gislason and Arnorsson, 1993), clogging by fine fragments (e.g. Kendrick et al., 2016) and secondary  
681 mineral precipitation (e.g. Curewitz and Karson, 1997). Such descriptions are the subject of ongoing  
682 work as part of the international IDDP and KMT projects.

683

## 684 **5 Conclusions**

685 This experimental study describes the permeability and storage capacity of the lithologies found  
686 within the Krafla reservoir. We find that each lithology exhibits a wide range of porosity and  
687 permeability; both of which are found to decrease nonlinearly with effective pressure – an effect  
688 which is more pronounced in samples with significant presence of fractures. We tested the influence of  
689 pressure oscillations, thermal stressing and fracturing on fluid flow in these rocks. We found that  
690 pressurisation/ depressurisation cycles leads to the progressive shutting of micro-fractures, which  
691 result in an overall permeability decrease of the rocks, though our experiments fluctuated pore  
692 pressure at values significantly lower than confinement, and we postulate that the effect may be  
693 reversed if pore pressure locally exceeded confining pressure. Thermal stimulation (especially when  
694 thermal shocks are caused by water) results in an increase of the permeability of rocks which are  
695 originally devoid of significant micro-fractures; however, fractured rocks remain largely unaffected by  
696 thermal stressing. Imparting a single macro-fracture increases the permeability of a rock at low  
697 effective pressure, but as confinement increases, the fracture begins to close and permeability trends  
698 towards that of the intact rock; imparting a second orthogonal fracture offers only a slightly higher  
699 increase in permeability of the rocks, but increases the possibility of offset along the fractures and thus

700 the persistence of high permeability under confinement. Where the fracture was slightly offset, or  
701 where fine fragments lodged themselves in the fracture, obstruction from closure at high effective  
702 pressure resulted in high, relatively pressure-independent permeabilities. The data suggests that when  
703 thermo-mechanically stimulating a reservoir, efforts should be made to generate fractures orthogonal  
704 to primary local faults and fractures, or at low angle to principal stresses in order to increase gap  
705 opening at their intersections and favour fluid flow in the hydrothermal system. These findings support  
706 the use of proppants, such as non-reactive granular materials, to open fractures and ensure efficient  
707 fluid flow in production wells.

708

## 709 **6 Acknowledgements**

710 This study has been partially financed by research funds from Landsvirkjun National Power Company  
711 of Iceland as well as a scholarship from the Institute for Risk and Uncertainty at the University of  
712 Liverpool and the European Research Council Starting Grant on Strain Localisation in Magma (SLiM,  
713 no. 306488). We wish to thank Dr. M.J. Heap and an anonymous reviewer for constructive comments  
714 as well as A. Lamur for fruitful discussions.

- 716 Alam, A.K.M.B., Niioka, M., Fujii, Y., Fukuda, D. and Kodama, J.-i., 2014. Effects of confining  
717 pressure on the permeability of three rock types under compression. *International Journal of*  
718 *Rock Mechanics and Mining Sciences*, 65: 49-61.
- 719 Aqai, A.R. and Zarrouk, S., 2011. Permeability enhancement of conventional geothermal wells, New  
720 Zealand Geothermal Workshop, Auckland, New Zealand.
- 721 Ashwell, P.A., Kendrick, J.E., Lavallée, Y., Kennedy, B.M., Hess, K.U., von Aulock, F.W.,  
722 Wadsworth, F.B., Vasseur, J. and Dingwell, D.B., 2015. Permeability of compacting porous  
723 lavas. *Journal of Geophysical Research: Solid Earth*, 120(3): 2014JB011519.
- 724 Austin-Erickson, A., Buttner, R., Dellino, P., Ort, M.H. and Zimanowski, B., 2008. Phreatomagmatic  
725 explosions of rhyolitic magma: Experimental and field evidence. *Journal of Geophysical*  
726 *Research-Solid Earth*, 113(B11).
- 727 Axelsson, G., Egilson, T. and Gylfadottir, S.S., 2014. Modelling of temperature conditions near the  
728 bottom of well IDDP-1 in Krafla, Northeast Iceland. *Geothermics*, 49: 49-57.
- 729 Bodvarsson, G.S., Pruess, K., Stefansson, V. and Eliasson, E.T., 1984. The Krafla Geothermal Field,  
730 Iceland: 2. The Natural State of the System Water Resource research, 20(11): 14.
- 731 Brace, W.F., 1980. Permeability of crystalline and argillaceous rocks. *International Journal of Rock*  
732 *Mechanics and Mining Sciences*, 17(5): 241-251.
- 733 Brace, W.F., Walsh, J.B. and Frangos, W.T., 1968. Permeability of granite under high pressure.  
734 *Journal of Geophysical Research*, 73(6): 2225-2236.
- 735 Brinton, D., McLin, K. and Moore, J., 2011. The chemical stability of Bauxite and quartz sand  
736 proppants under geothermal conditions, 36th Stanford Geothermal workshop on Geothermal  
737 Reservoir Engineering, Stanford, California.
- 738 Carlino, S., Somma, R., Troise, C. and De Natale, G., 2012. The geothermal exploration of Campanian  
739 volcanoes: Historical review and future development. *Renewable & Sustainable Energy*  
740 *Reviews*, 16(1): 1004-1030.
- 741 Curewitz, D. and Karson, J.A., 1997. Structural settings of hydrothermal outflow: Fracture  
742 permeability maintained by fault propagation and interaction. *Journal of Volcanology and*  
743 *Geothermal Research*, 79(3-4): 149-168.
- 744 Darcy, H., 1856. *Les fontaines publiques de la ville de Dijon*. Dalmont, Paris.
- 745 Darcy, H., 1857. *Recherches expérimentales relatives au mouvement de l'eau dans les tuyaux*. Mallet-  
746 Bachelier, École impériale polytechnique de Paris.
- 747 Darling, W.G. and Armannsson, H., 1989. Stable isotopic aspects of fluid-flow in the Krafla,  
748 Namafjall and Theistareykir geothermal systems of Northeast Iceland. *Chemical Geology*,  
749 76(3-4): 197-213.
- 750 Degraff, J.M. and Aydin, A., 1993. Effect of thermal regime on growth increment and spacing of  
751 contraction joints in basaltic lava. *J. Geophys. Res.-Solid Earth*, 98(B4): 6411-6430.
- 752 Edmonds, M. and Herd, R.A., 2007. A volcanic degassing event at the explosive-effusive transition.  
753 *Geophys. Res. Lett.*, 34(21): L21310.
- 754 Eggertsson, G.H., Lavallée, Y., Kendrick, J.E., Lamur, A. and Markússon, S., 2016. Enhancing  
755 permeability by multiple fractures in the Krafla geothermal reservoir, Iceland, European  
756 Geothermal Congress. European Geothermal Congress, Strasbourg.
- 757 Eichelberger, J.C., Carrigan, C.R., Westrich, H.R. and Price, R.H., 1986. Non-explosive silicic  
758 volcanism. *Nature*, 323(6089): 598-602.
- 759 Einarsson, P., 1978. S-wave shadows in the Krafla caldera in NE Iceland: evidence for a magma  
760 chamber in the crust. *Bulletin of Volcanology*, 41(3): 8.
- 761 Einarsson, P., 1991. The Krafla rifting episode 1975–1989 (Umbrotin við Kröflu 1975-89 in  
762 Icelandic). *Hið íslenska náttúrufræðifélag*, Reykjavík, 43 pp.
- 763 Elders, W.A., Fridleifsson, G.O. and Palsson, B., 2014. Iceland Deep Drilling Project: The first well,  
764 IDDP-1, drilled into magma Preface. *Geothermics*, 49: 1-1.
- 765 Elders, W.A., Frioleifsson, G.O., Zierenberg, R.A., Pope, E.C., Mortensen, A.K., Guomundsson, A.,  
766 Lowenstern, J.B., Marks, N.E., Owens, L., Bird, D.K., Reed, M., Olsen, N.J. and Schiffman,  
767 P., 2011. Origin of a rhyolite that intruded a geothermal well while drilling at the Krafla  
768 volcano, Iceland. *Geology*, 39(3): 231-234.

769 Farquharson, J., Heap, M.J., Varley, N.R., Baud, P. and Reuschle, T., 2015. Permeability and porosity  
770 relationships of edifice-forming andesites: A combined field and laboratory study. *Journal of*  
771 *Volcanology and Geothermal Research*, 297: 52-68.

772 Farquharson, J.I., Wadsworth, F.B., Heap, M.J. and Baud, P., 2017. Time-dependent permeability  
773 evolution in compacting volcanic fracture systems and implications for gas overpressure.  
774 *Journal of Volcanology and Geothermal Research*, 339: 81-97.

775 Fournier, R.O., 1999. Hydrothermal processes related to movement of fluid from plastic into brittle  
776 rock in the magmatic-epithermal environment. *Economic Geology and the Bulletin of the*  
777 *Society of Economic Geologists*, 94(8): 1193-1211.

778 Fridleifsson, G.O., Elders, W.A. and Albertsson, A., 2014. The concept of the Iceland deep drilling  
779 project. *Geothermics*, 49: 2-8.

780 Gallois, R., 2007. The formation of the hot springs at Bath Spa, UK. *Geological Magazine*, 144(4):  
781 741-747.

782 Ghassemi, A., 2012. A Review of Some Rock Mechanics Issues in Geothermal Reservoir  
783 Development. *Geotechnical and Geological Engineering*, 30(3): 647-664.

784 Gislason, S.R. and Arnorsson, S., 1993. Dissolution of primary basaltic minerals in natural waters:  
785 saturation state and kinetics. *Chemical Geology*, 105(1-3): 117-135.

786 Grant, M.A., Clearwater, J., Quinão, J., Bixley, P.F. and Le Brun, M., 2013. Thermal stimulation of  
787 geothermal wells: a review of field data, *Proceedings*.

788 Gudmundsson, A., 1995. Infrastructure and mechanics of volcanic systems in Iceland. *Journal of*  
789 *Volcanology and Geothermal Research*, 64(1-2): 1-22.

790 Gudmundsson, M.T., Larsen, G., Hoskuldsson, A. and Gylfason, A.G., 2008. Volcanic hazards in  
791 Iceland. *Jokull*, 58: 251-268.

792 Guðmundsson, Á., 2001. An expansion of the Krafla Power Plant from 30 to 60 MWe - Geothermal  
793 considerations. *Geothermal Resources council transactions*, 25: 6.

794 Hansell, A. and Oppenheimer, C., 2004. Health hazards from volcanic gases: A systematic literature  
795 review. *Archives of Environmental Health*, 59(12): 628-639.

796 Heap, M., Xu, T. and Chen, C.-f., 2014a. The influence of porosity and vesicle size on the brittle  
797 strength of volcanic rocks and magma. *Bulletin of Volcanology*, 76(9): 1-15.

798 Heap, M.J., Farquharson, J.I., Baud, P., Lavalée, Y. and Reuschle, T., 2015a. Fracture and  
799 compaction of andesite in a volcanic edifice. *Bulletin of Volcanology*, 77(6).

800 Heap, M.J. and Kennedy, B.M., 2016. Exploring the scale-dependent permeability of fractured  
801 andesite. *Earth and Planetary Science Letters*, 447: 139-150.

802 Heap, M.J., Kennedy, B.M., Pernin, N., Jacquemard, L., Baud, P., Farquharson, J.I., Scheu, B.,  
803 Lavalée, Y., Gilg, H.A., Letham-Brake, M., Mayer, K., Jolly, A.D., Reuschle, T. and  
804 Dingwell, D.B., 2015b. Mechanical behaviour and failure modes in the Whakaari (White  
805 Island volcano) hydrothermal system, New Zealand. *Journal of Volcanology and Geothermal*  
806 *Research*, 295: 26-42.

807 Heap, M.J., Kolzenburg, S., Russell, J.K., Campbell, M.E., Welles, J., Farquharson, J.I. and Ryan, A.,  
808 2014b. Conditions and timescales for welding block-and-ash flow deposits. *Journal of*  
809 *Volcanology and Geothermal Research*, 289: 202-209.

810 Heap, M.J., Mollo, S., Vinciguerra, S., Lavallée, Y., Hess, K.U., Dingwell, D.B., Baud, P. and Iezzi,  
811 G., 2013. Thermal weakening of the carbonate basement under Mt. Etna volcano (Italy):  
812 Implications for volcano instability. *Journal of Volcanology and Geothermal Research*, 250:  
813 42-60.

814 Heap, M.J., Russell, J.K. and Kennedy, L.A., 2016. Mechanical behaviour of dacite from Mount St.  
815 Helens (USA): A link between porosity and lava dome extrusion mechanism (dome or spine)?  
816 *Journal of Volcanology and Geothermal Research*, 328: 159-177.

817 Hjartardottir, A.R., Einarsson, P., Bramham, E. and Wright, T.J., 2012. The Krafla fissure swarm,  
818 Iceland, and its formation by rifting events. *Bulletin of Volcanology*, 74(9): 2139-2153.

819 Hofmann, H., Blocher, G., Milsch, H., Babadagli, T. and Zimmermann, G., 2016. Transmissivity of  
820 aligned and displaced tensile fractures in granitic rocks during cyclic loading. *International*  
821 *Journal of Rock Mechanics and Mining Sciences*, 87: 69-84.

822 Ingason, K., Kristjansson, V. and Einarsson, K., 2014. Design and development of the discharge  
823 system of IDDP-1. *Geothermics*, 49: 58-65.



824 Jansen, J.D., 2011. Adjoint-based optimization of multi-phase flow through porous media - A review.  
825 Computers & Fluids, 46(1): 40-51.

826 Jouniaux, L., Bernard, M.L., Zamora, M. and Pozzi, J.P., 2000. Streaming potential in volcanic rocks  
827 from Mount Pelee. Journal of Geophysical Research-Solid Earth, 105(B4): 8391-8401.

828 Kantha, L.H., 1981. Basalt fingers - Origin of columnar joints. Geological Magazine, 118(3): 251-&.

829 Kendrick, J.E., Lavallee, Y., Varley, N.R., Wadsworth, F.B., Lamb, O.D. and Vasseur, J., 2016.  
830 Blowing Off Steam: Tuffisite Formation As a Regulator for Lava Dome Eruptions. Frontiers  
831 in Earth Science, 4.

832 Kendrick, J.E., Lavallée, Y., Hess, K.U., Heap, M.J., Gaunt, H.E., Meredith, P.G. and Dingwell, D.B.,  
833 2013. Tracking the permeable porous network during strain-dependent magmatic flow.  
834 Journal of Volcanology and Geothermal Research, 260: 117-126.

835 Klug, C. and Cashman, K.V., 1996. Permeability development in vesiculating magmas: Implications  
836 for fragmentation. Bulletin of Volcanology, 58(2-3): 87-100.

837 Kolzenburg, S., Heap, M.J., Lavallée, Y., Russell, J.K., Meredith, P.G. and Dingwell, D.B., 2012.  
838 Strength and permeability recovery of tuffisite-bearing andesite. Solid Earth, 3(2): 191-198.

839 Koudina, N., Garcia, R.G., Thovert, J.F. and Adler, P.M., 1998. Permeability of three-dimensional  
840 fracture networks. Physical Review E, 57(4): 4466-4479.

841 Kushnir, A.R.L., Martel, C., Bourdier, J.-L., Heap, M.J., Reuschlé, T., Erdmann, S., Komorowski, J.-  
842 C. and Cholikh, N., 2016. Probing permeability and microstructure: Unravelling the role of a  
843 low-permeability dome on the explosivity of Merapi (Indonesia). Journal of Volcanology and  
844 Geothermal Research, 316: 56-71.

845 Kushnir, A.R.L., Martel, C., Champallier, R. and Wadsworth, F.B., 2017. Permeability Evolution in  
846 Variably Glassy Basaltic Andesites Measured Under Magmatic Conditions. Geophysical  
847 Research Letters, In Press.

848 Lamur, A., Kendrick, J.E., Eggertsson, G.H., Wall, R.J., Ashworth, J.D. and Lavallee, Y., 2017. The  
849 permeability of fractured rocks in pressurised volcanic and geothermal systems. Scientific  
850 Reports, 7.

851 Lamur, A.K., Jackie E., Wadsworth, F. and Lavallée, Y., In review. Timescales of fracture healing and  
852 strength recovery in magmatic liquids. Geology.

853 Lavallée, Y., Benson, P.M., Heap, M.J., Hess, K.U., Flaws, A., Schillinger, B., Meredith, P.G. and  
854 Dingwell, D.B., 2013. Reconstructing magma failure and the degassing network of dome-  
855 building eruptions. Geology, 41.

856 Lavallée, Y., Meredith, P.G., Dingwell, D.B., Hess, K.U., Wassermann, J., Cordonnier, B., Gerik, A.  
857 and Kruhl, J.H., 2008. Seismogenic lavas and explosive eruption forecasting. Nature,  
858 453(7194): 507-510.

859 Legarth, B., Huenges, E. and Zimmermann, G., 2005. Hydraulic fracturing in a sedimentary  
860 geothermal reservoir: Results and implications. International Journal of Rock Mechanics and  
861 Mining Sciences, 42(7-8): 1028-1041.

862 McClure, M.W. and Horne, R.N., 2014. An investigation of stimulation mechanisms in Enhanced  
863 Geothermal Systems. International Journal of Rock Mechanics and Mining Sciences, 72: 242-  
864 260.

865 Miller, S.A., 2015. Modeling enhanced geothermal systems and the essential nature of large-scale  
866 changes in permeability at the onset of slip. Geofluids, 15(1-2): 338-349.

867 Milsch, H., Hofmann, H. and Blocher, G., 2016. An experimental and numerical evaluation of  
868 continuous fracture permeability measurements during effective pressure cycles. International  
869 Journal of Rock Mechanics and Mining Sciences, 89: 109-115.

870 Mock, J.E., Tester, J.W. and Wright, P.M., 1997. Geothermal energy from the earth: Its potential  
871 impact as an environmentally sustainable resource. Annual Review of Energy and the  
872 Environment, 22: 305-356.

873 Mortensen, A.K., Egilson, P., Gautason, B., Arnadóttir, S. and Gudmundsson, A., 2014. Stratigraphy,  
874 alteration mineralogy, permeability and temperature conditions of well IDDP-1, Krafla, NE-  
875 Iceland. Geothermics, 49: 31-41.

876 Mortensen, A.K., Guðmundsson, Á., Steingrímsson, B., Sigmundsson, F., Axelsson, G., Ármannsson,  
877 H., Björnsson, H., Ágústsson, K., Sæmundsson, K., Ólafsson, M., Karlsdóttir, R.,  
878 Halldórsdóttir, S. and Hauksson, T., 2015. The Krafla Geothermal System Research summary  
879 and conceptual model revision, Landsvirkjun, Reykjavík.

880 Mueller, S., Melnik, O., Spieler, O., Scheu, B. and Dingwell, D.B., 2005. Permeability and degassing  
881 of dome lavas undergoing rapid decompression: An experimental determination. *Bulletin of*  
882 *Volcanology*, 67(6): 526-538.

883 Murphy, H.D., Tester, J.W., Grigsby, C.O. and Potter, R.M., 1981. Energy extraction from fractured  
884 geothermal reservoirs in low-permeability crystalline rock. *Journal of Geophysical Research*,  
885 86(NB8): 7145-7158.

886 Nara, Y., Meredith, P.G., Yoneda, T. and Kaneko, K., 2011. Influence of macro-fractures and micro-  
887 fractures on permeability and elastic wave velocities in basalt at elevated pressure.  
888 *Tectonophysics*, 503.

889 Nara, Y., Morimoto, K., Hiroyoshi, N., Yoneda, T., Kaneko, K. and Benson, P.M., 2012. Influence of  
890 relative humidity on fracture toughness of rock: implications for subcritical crack growth. *Int J*  
891 *Solids Struct*, 49.

892 Okumura, S. and Sasaki, O., 2014. Permeability reduction of fractured rhyolite in volcanic conduits  
893 and its control on eruption cyclicality. *Geology*, 42(10): 843-846.

894 Palsson, B., Holmgeirsson, S., Gudmundsson, A., Boasson, H.A., Ingason, K., Sverrisson, H. and  
895 Thorhallsson, S., 2014. Drilling of the well IDDP-1. *Geothermics*, 49: 23-30.

896 Pearson, C., 1981. THE RELATIONSHIP BETWEEN MICROSEISMICITY AND HIGH PORE  
897 PRESSURES DURING HYDRAULIC STIMULATION EXPERIMENTS IN LOW  
898 PERMEABILITY GRANITIC-ROCKS. *Journal of Geophysical Research*, 86(NB9): 7855-  
899 7864.

900 Perez-Flores, P., Wang, G., Mitchell, T.M., Meredith, P.G., Nara, Y., Sarkar, V. and Cembrano, J.,  
901 2017. The effect of offset on fracture permeability of rocks from the Southern Andes Volcanic  
902 Zone, Chile. *Journal of Structural Geology*, 104: 142-158.

903 Rozhko, A.Y., Podladchikov, Y.Y. and Renard, F., 2007. Failure patterns caused by localized rise in  
904 pore-fluid overpressure and effective strength of rocks. *Geophysical Research Letters*, 34(22).

905 Saar, M.O. and Manga, M., 1999. Permeability-porosity relationship in vesicular basalts. *Geophys Res*  
906 *Lett*, 26.

907 Schaefer, L.N., Kendrick, J.E., Lavallée, Y., Oommen, T. and Chigna, G., 2015. Geomechanical rock  
908 properties of a basaltic volcano. *Frontiers in Earth Science*, 3.

909 Scott, S., Driesner, T. and Weis, P., 2015. Geologic controls on supercritical geothermal resources  
910 above magmatic intrusions. *Nature Communications*, 6.

911 Siratovich, P.A., Heap, M.J., Villeneuve, M.C., Cole, J.W. and Reuschlé, T., 2014. Physical property  
912 relationships of the Rotokawa Andesite, a significant geothermal reservoir rock in the Taupo  
913 Volcanic Zone, New Zealand. *Geothermal Energy*, 2(1): 1-31.

914 Siratovich, P.A., Villeneuve, M.C., Cole, J.W., Kennedy, B.M. and Begue, F., 2015a. Saturated  
915 heating and quenching of three crustal rocks and implications for thermal stimulation of  
916 permeability in geothermal reservoirs. *International Journal of Rock Mechanics and Mining*  
917 *Sciences*, 80: 265-280.

918 Siratovich, P.A., von Aulock, F.W., Y., L., J.W., C., B.M., K. and M.C., V., 2015b. Thermoelastic  
919 properties of the Rotokawa Andesite: a geothermal reservoir constraint. *Journal of*  
920 *Volcanology and Geothermal Research* 301.

921 Stimac, J.A., Powell, T.S. and Golla, G.U., 2004. Porosity and permeability of the Tiwi geothermal  
922 field, Philippines, based on continuous and spot core measurements. *Geothermics*, 33.

923 Strehlow, K., Gottsmann, J.H. and Rust, A.C., 2015. Poroelastic responses of confined aquifers to  
924 subsurface strain and their use for volcano monitoring. *Solid Earth*, 6(4): 1207-1229.

925 Sæmundsson, K., 1991. Geology of the Krafla Volcanic system (Jarðfræði Kröflukerfisins in  
926 Icelandic). In: A. Garðarsson and Á. Einarsson (Editors), *Náttúra Mývatns. Hið íslenska*  
927 *náttúrufræðifélag, Reykjavík*, pp. 24-95.

928 Tanikawa, W. and Shimamoto, T., 2009. Comparison of Klinkenberg-corrected gas permeability and  
929 water permeability in sedimentary rocks. *International Journal of Rock Mechanics and Mining*  
930 *Sciences*, 46(2): 229-238.

931 Tiwari, G.N. and Ghosal, M.K., 2005. *Renewable Energy Resources: Basic Principles and*  
932 *Applications*. Alpha Science International.

933 Tomac, I. and Gutierrez, M., 2017. Coupled hydro-thermo-mechanical modeling of hydraulic  
934 fracturing in quasi-brittle rocks using BPM-DEM. *Journal of Rock Mechanics and*  
935 *Geotechnical Engineering*, 9(1): 92-104.

- 936 Tuffen, H., Dingwell, D.B. and Pinkerton, H., 2003. Repeated fracture and healing of silicic magma  
937 generate flow banding and earthquakes? *Geology*, 31(12): 1089-1092.
- 938 Violay, M., Gibert, B., Mainprice, D., Evans, B., Dautria, J.-M., Azais, P. and Pezard, P., 2012. An  
939 experimental study of the brittle-ductile transition of basalt at oceanic crust pressure and  
940 temperature conditions. *Journal of geophysical reserach*, 117.
- 941 Walsh, J.B., 1981. Effect of pore pressure and confining pressure on fracture permeability.  
942 *International Journal of Rock Mechanics and Mining Sciences & Geomechanics Abstracts*,  
943 18(5): 429-435.
- 944 Wong, T.-f. and Baud, P., 2012. The brittle-ductile transition in porous rock: A review. *Journal of*  
945 *Structural Geology*, 44: 25-53.
- 946 Zang, A.N., Oye, V., Jousset, P., Deichmann, N., Gritto, R., McGarr, A., Majer, E. and Bruhn, D.,  
947 2014. Analysis of induced seismicity in geothermal reservoirs - An overview. *Geothermics*,  
948 52: 6-21.
- 949 Zhang, J.X., Wong, T.F. and Davis, D.M., 1990. MICROMECHANICS OF PRESSURE-INDUCED  
950 GRAIN CRUSHING IN POROUS ROCKS. *Journal of Geophysical Research-Solid Earth and*  
951 *Planets*, 95(B1): 341-352.
- 952 Zierenberg, R.A., Schiffman, P., Barfod, G.H., Leshner, C.E., Marks, N.E., Lowenstern, J.B.,  
953 Mortensen, A.K., Pope, E.C., Bird, D.K., Reed, M.H., Friðleifsson, G.Ó. and Elders, W.A.,  
954 2013. Composition and origin of rhyolite melt intersected by drilling in the Krafla geothermal  
955 field, Iceland. *Contributions to Mineralogy and Petrology*, 165(2): 327-347.
- 956 Zimmermann, G., Blocher, G., Reinicke, A. and Brandt, W., 2011. Rock specific hydraulic fracturing  
957 and matrix acidizing to enhance a geothermal system - Concepts and field results.  
958 *Tectonophysics*, 503(1-2): 146-154.
- 959 Zimmermann, G., Tischner, T., Legarth, B. and Huenges, E., 2009. Pressure-dependent Production  
960 Efficiency of an Enhanced Geothermal System (EGS): Stimulation Results and Implications  
961 for Hydraulic Fracture Treatments. *Pure and Applied Geophysics*, 166(5-7): 1089-1106.
- 962 Ármannsson, H., 1989. Gas changes in the Krafla geothermal system, Iceland. *Water-rock interaction*,  
963 76(3-4): 19.
- 964